A B cell actomyosin arc network couples integrin co-stimulation to mechanical force-dependent immune synapse formation

Jia C. Wang[1], Yang-In Yim[1], Xufeng Wu[2], Valentin Jaumouillé[1], Clare M. Waterman[1], John H. Kehrl[3], and John A. Hammer[1,4]

[1] Cell and Developmental Biology Center, National Heart, Lung and Blood Institute, National Institutes of Health, Bethesda MD 20892

[2]Light Microscopy Core, National Heart, Lung and Blood Institute, National Institutes of Health, Bethesda MD 20892

[3]B Cell Molecular Immunology Section, National Institute of Allergy and Infectious Disease, National Institutes of Health, Bethesda MD 20892

[4]Author for correspondence: hammerj@nhlbi.nih.gov

Abstract

B-cell activation and immune synapse (IS) formation with membrane-bound antigens are actin-dependent processes that scale positively with the strength of antigen-induced signals. Importantly, ligating the B-cell integrin, LFA-1, with ICAM-1 promotes IS formation when antigen is limiting. Whether the actin cytoskeleton plays a specific role in integrin-dependent IS formation is unknown. Here we show using super-resolution imaging of primary B cells that LFA-1: ICAM-1 interactions promote the formation of an actomyosin network that dominates the B-cell IS. This network is created by the formin mDia1, organized into concentric, contractile arcs by myosin 2A, and flows inward at the same rate as B-cell receptor (BCR): antigen clusters. Consistently, individual BCR microclusters are swept inward by individual actomyosin arcs. Under conditions where integrin is required for synapse formation, inhibiting myosin impairs synapse formation, as evidenced by reduced antigen centralization, diminished BCR signaling, and defective signaling protein distribution at the synapse. Together, these results argue that a contractile actomyosin arc network plays a key role in the mechanism by which LFA-1 co-stimulation promotes B-cell activation and IS formation.

Introduction

BCR engagement with cognate antigen triggers striking changes in B cell physiology that promote B cell activation, immune synapse (IS) formation, and B cell effector functions (1-3). These changes include dramatic increases in actin filament assembly and dynamics that are thought to drive IS formation in B cells engaged with membrane-bound antigen (1-4). For B cells *in vivo*, this usually involves interactions with antigen bound to the surface of an antigen-presenting cell (APC) (4-6), although activating surfaces such as antigen-coated glass and planar lipid bilayers containing freely-diffusing antigen are used to mimic these *in vivo* interactions. IS formation in these contexts is initiated by the formation of a radially-symmetric, Arp2/3 complex-dependent branched actin network at the outer edge of the IS (i.e. in the distal supramolecular activation cluster or dSMAC) (7, 8). This lamellipodia-like actin network drives the spreading of the B cell across the antigen-coated surface, thereby promoting BCR: antigen interactions (3, 9). Once the B cell is fully spread, the continued polymerization of branched actin at the outer edge of the dSMAC generates a centripetal or retrograde flow of actin that drives the movement of BCR: antigen clusters (10-12) towards the center of the synapse (i.e. to the central SMAC or cSMAC) (8, 13). This centripetal actin flow, combined with an overall contraction of the B cell, is thought to be responsible for the transport of BCR: antigen clusters to the center of the maturing synapse (13). Importantly, this process of antigen centralization is required for robust BCR signaling (3, 11, 14), and is thought to be a prerequisite for antigen internalization by follicular B cells (15-17).

Antigen-induced IS formation scales with the strength of antigen-induced signals such that IS formation and B cell activation are attenuated when membrane-bound antigen binds the BCR weakly or is presented at low density. Importantly, co-stimulatory signals can promote IS formation and B cell activation under both of these conditions (18, 19). Seminal work from Carrasco and colleagues showed that the B-cell integrin LFA-1, which binds the adhesion molecule ICAM-1 present on the surface of APCs (20, 21), serves as one such co-stimulatory signal (18). This conclusion was based on four key observations. First, B cells responded robustly to higher affinity membrane-bound antigens presented at high density whether or not ICAM-1 was present on the membrane. Second, the robust activation of B cells in response to antigens of all affinities increasingly required ICAM-1 in the membrane as the density of the antigen was lowered. Third, this co-stimulatory effect was most dramatic for weaker antigens. Finally, this latter effect was not observed in B cells lacking LFA-1. With regard to the underlying mechanism, IRM imaging suggested that LFA-1: ICAM-1 interactions, which were shown to concentrate in the medial portion of the synapse (i.e. the peripheral SMAC or pSMAC), lower the threshold for B cell activation by enhancing cell adhesion.

While the actin cytoskeleton clearly plays a central role in driving IS formation, whether it plays a specific role in integrin-dependent IS formation is unknown. This is an important question, as most B cell interactions with professional APCs presenting cognate antigen involve integrin ligation. Relevant to this question, the dendritic actin network occupying the outer dSMAC ring, which is thought to be the main driver of IS formation, has been observed primarily in cells that received antigen stimulation alone, and almost exclusively in immortalized B cell lines (13, 22-25). It is not known, therefore, whether integrin-co-stimulation alters the organization and/or dynamics of actin at the B-cell IS. Moreover, we are only just beginning to elucidate the organization and dynamics of synaptic actin networks formed by primary B cells. Here we show that LFA-1: ICAM-1 interactions in primary B cells stimulate the formation of a contractile actomyosin arc network that occupies the pSMAC portion of the synapse. This actomyosin network represents the major actin structure at the IS of primary B cells receiving integrin co-stimulation, and its dynamics drive antigen centralization by sweeping antigen centripetally. Importantly, under conditions of limiting antigen, where integrin co-stimulation is required for IS formation, blocking the contractility of this pSMAC network inhibits IS formation and BCR signaling. Finally, we show that germinal center (GC) B cells can also create this actomyosin structure, suggesting that it contributes to the process of antibody affinity maturation. Together, our data demonstrate that a contractile actomyosin arc network created downstream of integrin ligation plays a major role in the mechanism by which integrin co-stimulation promotes B cell activation and IS formation when antigen is limiting. Importantly, these findings highlight the need for including integrin co-stimulation when examining the role of actin during B cell activation, especially under physiologically relevant conditions.

Results

Integrin co-stimulation promotes the formation of an actin arc network in the pSMAC

To investigate the possibility that LFA-1 ligation might promote B cell activation by triggering a significant change in synaptic actin organization, we imaged F-actin at ISs formed by primary mouse B cells on glass surfaces coated with either anti-IgM or anti-IgM plus ICAM-1. F-actin was visualized using GFP-F-Tractin, a dynamic reporter for F-actin (26, 27), and two super-resolution imaging modalities: Airyscan (*xy* resolution ~140 nm) and total internal reflection-structured illumination (TIRF-SIM; *xy* resolution ~100 nm). Individual video frames of anti-IgM-engaged B cells using both imaging modalities (Fig. 1A, B), together with the corresponding movies (Movies 1A and 1B), revealed a thin, bright, highly-dynamic outer rim of F-actin (white arrows in Fig. 1A, B) that likely corresponds to the branched actin network comprising the dSMAC (13, 22, 25). Both modalities (but especially TIRF-SIM) showed that the F-actin present inside this outer dSMAC rim is composed of a highly disorganized mixture of short actin filaments/fibers and actin foci (blue brackets in Fig. 1A, B). In sharp contrast, individual video frames of anti-IgM+ICAM-1-engaged B cells using both modalities (Fig. 1C, D), together with the corresponding movies (Movies 2A and 2B), showed a highly organized network inside the outer dSMAC rim (i.e. in the pSMAC) that is comprised of concentric actin arcs (blue brackets and red arrows in Fig. 1C, D). The difference in synaptic actin organization between anti-IgM-engaged B cells and anti-IgM+ICAM-1-engaged B cells is very evident in enlarged TIRF-SIM images. While it is challenging to define SMAC boundaries and any pattern of F-actin organization in the pSMAC of B cells engaged with anti-IgM alone (Fig. 1E1, E2), SMAC boundaries and pSMAC F-actin organization are both very distinct in B cells engaged using anti-IgM+ICAM-1 (Fig. 1F1, F2). Consistently, scoring B cells for the presence of a discernable actin arc network showed that the addition of ICAM-1 increases the percentage of such cells from ~30% to ~70% (Fig. 1G). Moreover, dynamic imaging showed that the arcs in cells engaged with anti-IgM alone are typically sparse and transient (Movies 1A and 1B), while those in cells engaged with both anti-IgM and ICAM-1 are dense and persistent (Movies 2A and 2B). Finally, measuring the percentage of total synaptic F-actin content within each SMAC (Fig. 1H), and the percentage of total IS footprint occupied by each SMAC (Fig. 1I), showed that the actin arc-containing pSMAC comprises the major actin network at the IS of primary B cells engaged using both anti-IgM and ICAM-1. Together, these results demonstrate that LFA-1 co-stimulation promotes the formation of a pSMAC actin arc network that dominates the B cell IS.

Linear actin filaments generated by the formin mDia1 at the outer edge of the synapse give rise to the pSMAC actin arc network

We next sought to define the origin of the actin arcs that comprise the pSMAC of B cells stimulated using both anti-IgM and ICAM-1. Primary B cells stimulated in this way exhibit small, actin-rich surface spikes at the outer synapse edge (Fig. 2A). Importantly, magnified images revealed that the actin within these spikes continues into the cytoplasm in the form of linear actin filaments (Fig. 2B1, B2). Moreover, tracing these linear actin filaments showed that they are contiguous with the pSMAC actin arcs (Fig. 2C1, C2; Movies 3A and 3B). These results argue that linear actin filaments nucleated at the plasma membrane at the outer edge of the synapse give rise to the actin arcs populating the pSMAC. While these results do not identify the specific nucleator involved, they do point to it being a member of the formin family based on the fact that the actin being made is linear and nucleated at the plasma membrane (28, 29). Consistent with this conjecture, and with the fact that formins incorporate fluorescent protein-labelled actin monomer into filaments poorly (26, 27, 30), we did not see fluorescent actin arcs in B cells expressing mEOS-labeled G-actin (Movie 4).

To test if a formin is indeed responsible for creating the pSMAC actin arc network, we used the pan-formin inhibitor SMIFH2 (31). Fig. 2D1 and 2D2, together with the line scan in Fig. 2E, show that the pSMAC actin arcs present in a representative primary B cell immediately before SMIFH1 addition (blue trace) had largely disappeared 6 minutes after adding SMIFH2 (red trace). Given recent concerns about the specificity of SMIFH2 (32), we used three different miRNAs to knock down the formin mDia1 in the lymphoma B cell line A20 (Fig. S1), which also forms pSMAC actin arcs when stimulated using anti-IgG+ICAM-1 (Fig. 1J1, J2; Movie 5A). mDia1 was chosen as the miRNA target as it is highly expressed in B cells (Immgen Database) and is largely responsible for making linear actin filaments in T cells (27). Compared to control A20 B cells (Fig. 2F1), representative B cells expressing each of the three miRNAs (Fig. 2F2-F4) were largely devoid of actin arcs. This difference was supported by quantitating the ratio of pSMAC to dSMAC F-actin (Fig. 2G), as well as the amount of F-actin in the pSMAC (Fig. 2H). Together, these results argue that the pSMAC actin arcs are indeed created by a formin, and that the formin mDia1 plays a major role.

To provide one final piece of evidence that the arcs are created by a formin, we imaged A20 B cells following the addition of the Arp2/3 inhibitor CK-666. The rationale for this experiment lies in the recent revelation that the two major consumers of actin monomer in cells, the Arp2/3 complex and formins, are always competing for a limiting pool of actin monomer (33-36). One consequence of this competition is that when one of these nucleators is inhibited, the actin structures created by the other nucleator get more robust because that nucleator now gets more monomer. For example, inhibiting the Arp2/3 complex promotes the formation of formin-dependent actin networks in both yeast and vertebrate cells (27, 33-36). Given this, and assuming that the arcs in B cells are formin-generated, then inhibiting the Arp2/3 complex in B cells should lead not only

to a diminution of the branched actin network in the dSMAC, but also to an amplification of the arc network in the pSMAC. Consistently, Figure S2A1/A2 (before CK-666 addition) and Figure S2A3/A4 (after CK-666 addition) together show that CK-666 addition leads not only to a reduction in the size of the dSMAC (red brackets), but also to an increase in arc content in the pSMAC (blue brackets). These changes were supported by measuring the percentage of total synaptic F-actin content residing within each SMAC (Fig. S2B), which revealed a significant shift away from dSMAC F-actin and toward pSMAC F-actin following CK-666 treatment. This shift was also reflected in measurements of total pSMAC F-actin content (Fig. S2C), the ratio of pSMAC to cSMAC F-actin content (Fig. S2D), and the ratio of pSMAC to cSMAC area (Fig. S2E). Taken together, these data argue strongly that linear actin filaments generated by the formin mDia1 at the outer edge of the synapse give rise to the pSMAC actin arc network.

Myosin 2A co-localizes with the actin arcs

Having established that ICAM-1 co-stimulation promotes the formin-dependent formation of actin arcs in the pSMAC, we asked how these arcs are organized into concentric structures. Formin-derived linear actin filaments are commonly organized into well-defined structures such as stress fibers, transverse arcs, and the contractile ring in dividing cells by bipolar filaments of the actin-based motor protein myosin 2 (37-39). We decided, therefore, to test whether myosin 2 co-localizes with the actin arcs and is required for their concentric organization.

To define the localization and dynamics of myosin 2 at the B cell IS, we used primary B cells isolated from a mouse in which GFP had been knocked into the N-terminus of the myosin 2A (M2A) heavy chain gene (40), as M2A is the only myosin 2 isoform expressed in B cells (Immgen Database). Individual video frames of these cells following transfection with Td-Tomato-F-Tractin and attachment to coverslips coated with anti-IgM and ICAM-1 revealed a dramatic co-localization between M2A and the actin arcs in the pSMAC (Fig. 3A1-A3; Movie 6). Magnified TIRF-SIM images show that the myosin signals align with actin arcs in a periodic fashion (Fig. 3A4) that resembles other myosin 2-rich, linear actin structures like stress fibers and the contractile ring (41). Moreover, these myosin signals exhibit the SIM signature for M2A bipolar filaments when M2A is GFP-labeled at its N-terminus (42), which is a pair of GFP puncta spaced ~300 nm apart (Fig. 3A5; 304 ± 32 nm; n = 230 filaments from 12 cells). The presence of M2A filaments in the medial portion of the synapse was also evident in primary B cells isolated from a mouse in which mCherry had been knocked into the N-terminus of M2A (Fig. S3A), in primary B cells that we genome edited using CRISPR to place GFP at the N-terminus of M2A (Fig. S3B), and in A20 B cells that we genome edited using CRISPR to place mScarleti at the N-terminus of M2A and then transfected with GFP-F-Tractin (Fig. S3C1-C3; Movie 5B). Finally, 3D-SIM images of A20 B cells that were fixed

and stained for M2A and actin showed that endogenous M2A also co-localizes with the actin arcs (Fig. S3D1-D3; note that the signature for M2A filaments using this antibody, which recognizes the C-terminus of M2A, is a single fluorescent punctum that corresponds to the center of an individual M2A filament (41, 43)). The extent of this colocalization was even clearer in enlarged images of immunostained cells (Fig. S3E1-E3), where line scans showed endogenous M2A coinciding with actin arcs (Fig. S3F). Together, these results show that the actin arc network in primary B cells receiving ICAM-1 co-stimulation is in fact an actomyosin arc network.

To gain insight into how the arcs become decorated with M2A filaments, we examined time lapse TIRF-SIM images of GFP-M2A knockin primary B cells expressing Td-Tomato F-Tractin. Individual video frames (Fig. 3B1-B6), as well as the corresponding movie (Movie 7), show that bipolar filaments of M2A begin to appear near the dSMAC: pSMAC boundary in association with the linear actin filaments/bundles exiting the dSMAC (white, yellow and fuchsia arrowheads mark such myosin filaments at time 0s in Fig. 3B1). As time progresses, these filaments move centripetally and undergo expansion into filament clusters (Fig. 3B1-B6; see also Movie 7). This expansion, in which individual myosin filaments expand into a small cluster of filaments, is presumably driven by the same sequential amplification pathway described previously for M2A filament assembly in Hela cells (42). Finally, the myosin filaments in these clusters begin to align with the arcs forming at the outer edge of the pSMAC, which then merge with the larger actomyosin arc network in the pSMAC (Fig. 3B1-B6). As all this is happening, new myosin filaments keep appearing near the dSMAC: pSMAC boundary to repeat the process (Fig. 3B2-B6; follow the blue, green and purple arrowheads).

Given that ICAM-1 co-stimulation promotes the formation of actin arcs, and that the arcs recruit M2A, ICAM-1 co-stimulation should also result in an increase in the amount of M2A at the IS. Consistently, primary GFP-M2A knockin B cells receiving both anti-IgM and ICAM-1 stimulation exhibited a greater amount of synaptic M2A than B cells receiving only anti-IgM stimulation (Fig. 3C-3E). Of note, this difference remained significant even after normalizing the M2A fluorescence for a small difference in the average cell-spread area under these two conditions (Fig. S3G1, G2).

Myosin 2A contractility is required for the concentric organization of the actin arcs and for integrin-dependent traction force

The organization of formin-generated linear actin filaments into well-defined structures is typically driven by the contractility of myosin 2 filaments (37, 38). Therefore, we asked if M2A contractility is required for the concentric organization of the pSMAC actin arcs by treating cells with para-nitroblebbistatin (pnBB), a blue light-insensitive version of the cell-permeable, small molecule myosin 2 inhibitor blebbistatin

(BB) that blocks myosin 2-based contractility by locking the myosin in its weak actin binding state (44). While control, DMSO-treated cells exhibited concentric actin arcs in their pSMAC as expected (Fig. 3F), cells treated with 25 μM pnBB displayed highly-disorganized, mesh-like actin arrays in their pSMAC (Fig. 3G). To quantify this defect in pSMAC actin organization, we used FibrilTool (45) to measure the anisotropy of actin filaments in the pSMAC. This tool measures how well structures of interest (here actin filaments) within a given region of interest (ROI; here the pSMAC) are arranged in parallel (anisotropy values range from 0 when the orientation of the structures is completely random to 1.0 when all of the structures are perfectly aligned/parallel to each other). To measure actin anisotropy in the radially-symmetric IS, we "linearized" pSMACs by dividing them into 10-12 trapezoid-shaped ROIs of similar size (Fig. S3H). As anticipated, the anisotropy values revealed a dramatic shift towards more disorganized pSMAC actin when B cells are treated with pnBB (Fig. 3H). Together, these results demonstrate that M2A contractility is indeed required for the concentric organization of the pSMAC actin arcs.

We used traction force microscopy in combination with pnBB to ask if integrin-dependent traction forces that B cells exert on a deformable substate require M2A contractility. As expected (46, 47), B cells engaged with substrate coated with anti-IgM and ICAM-1 generated significantly more traction force than B cells engaged with substrate coated with anti-IgM alone (Fig. S4A1, A2, B1, B2, D). Importantly, ICAM-1-dependent traction forces were completely abrogated by pre-treating the cells with pnBB (Fig. S4C1, C2, D), indicating that the generation of integrin-dependent traction forces requires M2A contractility. This requirement likely reflects pulling forces exerted by M2A on the substrate through LFA-1: ICAM-1 pairs, combined with the increase in M2A content at the synapse caused by ligating LFA-1 with ICAM-1, and the contribution that M2A-dependent pulling forces make in keeping LFA-1 in its open, active conformation (48-50). These results, together with the fact that integrin clusters are known to accumulate in the pSMAC portion of the B cell IS (18, 19), suggest a feed-forward relationship where integrin ligation promotes the formation of pSMAC actomyosin arcs, and the contractile forces exerted by these actomyosin arcs promote further integrin activation and robust adhesion in the pSMAC.

The actomyosin arc network in the pSMAC exhibits centripetal flow

Inward flows of cortical actin networks are thought to drive the transport of antigen receptor clusters to the center of maturing synapses in both T cells and B cells ((7, 36, 50); although see (51, 52)). For B cells, the clearest example of this to date is the demonstration that the centripetal flow of the branched actin network comprising the dSMAC propels BCR: antigen clusters towards the cSMAC (13). As a prelude to asking whether the actomyosin arcs comprising the pSMAC also contribute to antigen centralization, we asked if this contractile network exhibits centripetal flow. Kymograph

analyses of actin flow across synapses made by primary B cells expressing GFP-F-Tractin showed that their pSMAC actomyosin arc network indeed flows centripetally at 1.07 +/-0.07 µm/min, or about one third the rate of centripetal actin flow in the dSMAC (2.89 +/- 0.18 µm/min) (Fig. S5A1-A3). Similar results were obtained for A20 B cells (pSMAC rate: 0.97 +/- 0.13 µm/min; dSMAC rate: 3.16 +/- 0.35 µm/min) (Fig. S5B1-B3). Together, these results indicate that the actomyosin arcs could contribute along with the branched actin network in the dSMAC to the inward transport of BCR: antigen clusters.

Actomyosin arcs contribute to antigen centralization by sweeping BCR: antigen clusters inward

We used planar lipid bilayers (PLBs) to determine if the actomyosin arcs do in fact contribute to antigen centralization. As expected, primary B cells expressing GFP-F-Tractin readily formed actin arcs when PLBs contained both anti-IgM and ICAM-1 (Movie 8A), but not when they contained anti-IgM alone (Movie 8B). Also as expected, primary B cells engaged with PLBs containing fluorescent anti-IgM (red) and unlabeled ICAM-1 yielded mature synapses in which concentric actin arcs surrounded antigen accumulated in the cSMAC (Fig. 4A1-A3, white arrows). To obtain a holistic view of antigen centralization, we imaged antigen clusters in the dSMAC and pSMAC of primary B cells over time with the aim of correlating their rates of centripetal transport with the distinct rates of centripetal actin flow exhibited by these two IS zones (Movie 9). Tracking of single antigen microclusters showed that they moved inward at 2.36 +/- 1.1 µm/min and 1.03 +/- 0.3 µm/min across the dSMAC (red tracks) and pSMAC (green tracks), respectively (Fig. 4B and 4C). Importantly, these rates are very similar to the rates of centripetal actin flow across the dSMAC and pSMAC, respectively (Fig. S5A1-A3). Together, these observations argue that the pSMAC actomyosin arc network works together with the dSMAC branched actin network to drive antigen centralization.

To identify the mechanism by which the actomyosin arcs drive antigen centralization, we imaged F-actin and anti-IgM in the medial portion of forming synapses at high magnification using TIRF-SIM. Anti-IgM microclusters were seen to move across the pSMAC towards the cSMAC (which in the following images was in the down direction) while embedded in an arc network moving in the same direction (Movie 10). White lines in Movie 10 and in the corresponding still images in Fig. 4D1-D6 mark actin arcs that were sweeping an individual anti-IgM microcluster inward (Fig. 4E1-E6). Figure 4F shows the trajectory of this microcluster (temporally color-coded) as it moved towards the cSMAC. Finally, a kymograph of this trajectory (Fig. 4G) shows that several actin arcs contributed to the inward movement of this microcluster (areas bracketed in white), and that pauses in movement (areas bracketed in pink) occurred where no actin signal was immediately adjacent to the microcluster. Together, these results argue that individual actin arcs move individual BCR: antigen microclusters inward via a sweeping mechanism that likely depends on frictional coupling between the actin arc and the

microcluster (53-55). While arcs can slip past microclusters, the overall incidence of such slippage must be fairly small as the rate of inward antigen transport across the pSMAC (Fig. 4C) is not significantly slower than the rate of inward actin arc flow across the pSMAC (Fig. S5A3).

Integrin ligation-dependent IS formation requires myosin 2A contractility

B cells engaged with membrane-bound antigen at low density fail to centralize antigen unless their integrin LFA-1 is also engaged with ICAM-1 in the target membrane (18). As a prelude to investigating the myosin dependence of this integrin co-stimulatory effect, we sought to recapitulate these findings using primary B cells and PLBs containing varying amounts of mobile, fluorophore-labeled anti-IgM antibody in the presence or absence of unlabeled ICAM-1. Using this approach, we determined an amount of anti-IgM antibody that would not elicit robust antigen centralization in the absence of ICAM-1, but would in its presence. B cells exhibited robust antigen centralization/cSMAC formation over 10 minutes without the need for ICAM-1 when the PLB was loaded using a solution containing anti-IgM at a concentration of 2 μg/ml (hereafter referred to as “high density antigen”) (Fig. S6A1-A3). By contrast, B cells formed antigen microclusters across their synaptic interface but failed to centralize them over 10 minutes when the PLB was loaded using a solution containing anti-IgM at a concentration 0.15 μg/ml (hereafter referred to as “low or limiting density antigen”) (Fig. S6B1-B3). Importantly, when unlabeled ICAM-1 was included in these low-density antigen bilayers, B cells now exhibited robust antigen centralization/cSMAC formation (Fig. S6C1-C3). This co-stimulatory effect was supported by scoring antigen distribution as centralized, partially centralized or non-centralized (Fig. S6D1-D3 and E). It was also supported by scoring the percent of total synaptic antigen present within the cSMAC, which was defined by a circular area encompassing 20% of the entire synaptic interface and centered around the center of mass of the fluorescent antigen-containing pixels within the interface (Fig. S6F). Finally, it was supported by measuring the size of antigen clusters as a function of their distance from the center of the cSMAC (defined as above) (Fig. S6G). Specifically, B cells engaged with PLBs containing antigen at the limiting density and no ICAM-1 exhibited small antigen clusters (~0.3 μm^2) located roughly evenly across the synaptic interface (Fig. S6G, black trace), while B cells engaged with PLBs containing ICAM-1 in addition to antigen at the limiting density exhibited large antigen clusters (up to 3 μm^2), the largest of which were located at the center of the cSMAC (Fig. S6G, green trace). Of note, the total amount of antigen present at the synaptic interface was also greater for cells engaged with low density anti-IgM+ICAM-1 than for cells engaged with low density anti-IgM alone (Fig. S6H). Together, these results recapitulated a central aspect of the integrin co-stimulatory effect described by Carrasco *et al.* (18), and they established the specific conditions we used next to test the myosin dependence of this co-stimulatory effect.

To score the myosin dependence of the integrin co-stimulatory effect, we measured the ability of primary B cells treated with either vehicle control (DMSO) or pnBB to centralize antigen and form a cSMAC when engaged for 10 minutes with PLBs containing ICAM-1 and anti-IgM at the limiting density. While DMSO-treated cells exhibited robust antigen centralization/cSMAC formation (Fig. 5A1-A3), pnBB-treated cells failed to centralize antigen/create a cSMAC (Fig. 5B1-B3). Consistently, the actin arcs that surround centralized antigen in DMSO-treated cells (Fig. 5C1-C3; white arrows) were absent in pnBB-treated cells (Fig. 5D1-D3). The fact that myosin inhibition abrogates the integrin co-stimulatory effect was further supported by scoring antigen distribution in control and pnBB-treated cells as centralized, partially centralized or non-centralized (Fig. 5E), by scoring the percent of total synaptic antigen present within the cSMAC (Fig. 5F), and by measuring the size of antigen clusters as a function of their distance from the center of the cSMAC (Fig. 5G). Of note, the total amount of antigen present at the synaptic interface was also greater for cells treated with DMSO than for cells treated with pnBB (Fig. 5H). Together, these results show that the ability of integrin ligation to promote antigen centralization and cSMAC formation when antigen is limiting requires myosin contractility. This in turn argues that the contractile actomyosin arc network created downstream of integrin ligation plays an important role in the mechanism by which LFA-1 co-stimulation promotes B cell activation.

Finally, we were curious if the robust centralization of antigen that occurs in the absence of LFA-1 ligation when the density of antigen is high is also dependent on myosin contractility, at least to some extent. Indeed, we found that treatment with para-amino BB (paBB), a newer, slightly more water soluble version of BB (56), attenuated antigen centralization significantly even when the density of antigen was high (Fig. S6; see legend for details), although the magnitude of the inhibition was smaller than for B cells engaged with limiting antigen plus ICAM-1 (compare the results in Fig. S6 to the results in Fig. 5). We conclude, therefore, that M2A contractility potentiates antigen centralization when antigen density is high as well as when antigen density is low enough that LFA-1 co-stimulation becomes important for IS formation.

Myosin 2A contractility promotes BCR-dependent signaling

To measure the contribution that actomyosin arcs might make to BCR-dependent signaling, we determined the effect that pnBB has on the distribution and synaptic content of phosphorylated CD79a (P-CD79a), an early signaling molecule responsible for signal transduction downstream of BCR-antigen interaction (14, 57). Consistent with results above and with the known properties of CD79a, DMSO-treated primary B cells engaged for 10 minutes with PLBs containing ICAM-1 and limiting antigen and then fixed/stained for P-CD79a exhibited robust cSMAC formation, with P-CD79a and anti-IgM concentrated in the cSMAC (Fig. 6A1-A4). Also as expected, pnBB-treated B cells failed to form a clear cSMAC, resulting in CD79a and anti-IgM spread across the

synapse (Fig. 6B1-B4). Importantly, quantitation showed that pnBB-treated cells also exhibited a significant reduction relative to control cells in synaptic P-CD79a content (Fig. 6C). This defect was also seen after only 5 minutes on PLBs (Fig. S8A), and the defects at both time points were not due to differences between BB-treated cells and control cells in synaptic CD79a content (Fig. S8B).

To extend these results, we determined the effect that pnBB has on the distribution and synaptic content of phosphorylated CD19, an important co-receptor for the BCR that is responsible for PI3K activation (3, 58-60). DMSO-treated primary B cells engaged with PLBs as above exhibited robust cSMAC formation, with P-CD19 enriched at the outer edge of the IgM concentrated in the cSMAC (Fig. 6D1-D4). This enrichment of P-CD19 at the pSMAC/cSMAC boundary was confirmed by line scans of the fluorescence intensities for F-actin, anti-IgM and P-CD19 (Fig. 6G, see boxed pSMAC regions). In contrast to control cells, pnBB-treated B cells failed to concentrate anti-IgM at the center of the synapse, and P-CD19 staining was now spread across the synaptic interface (Fig. 6E1-E4 and H). Moreover, quantitation showed that pnBB-treated cells also exhibited a significant reduction relative to control cells in synaptic P-CD19 content (Fig. 6F) that was not due to a difference in synaptic CD19 content (Fig. S8C). Together, these results indicate that the actomyosin arcs promote BCR-dependent signaling.

Germinal center B cells can make actomyosin arcs and centralize antigen

Recent studies have presented evidence that germinal center (GC) B cells differ markedly from naive B cells with regard to the distribution and fate of antigen at mature synapses. Rather than concentrating antigen at the center of the synapse and using actomyosin force to extract it there, GC B cells accumulate antigen in clusters at the periphery of the synapse and use actomyosin force to extract it there (36, 61, 62). These and other results argue that GC B cells differ dramatically from naïve B cells with regard to the organization of actomyosin at their synapse. We wondered, however, if actomyosin arcs could be detected in mouse GC B cells using our imaging approaches. Consistently, TIRF-SIM imaging of mouse GC B cells isolated from the GFP-M2A knockin mouse that were stained with Cell Mask Deep Red and plated on coverslips coated with anti-IgM, anti-IgG and ICAM-1 revealed a subset of cells exhibiting enrichment of M2A filaments in the medial, pSMAC portion of the synapse (Movie 11), just as in naïve B cells. Moreover, these myosin filaments move centripetally (Movie 11) and co-localize with pSMAC actin arcs in phalloidin-stained samples (Fig. 7A1-A3, white arrows), just as in naive B cells. Importantly, scoring showed that about one third of GC B cells exhibit robust accumulation of M2A filaments in the pSMAC (Fig. 7B). Similar results were obtained when GFP-M2A knockin GC B cells were engaged for 10 minutes with PLBs containing fluorophore-labeled anti-IgM/IgG and unlabeled ICAM-1, and then

446 fixed and stained with phalloidin, where about one third of the cells exhibited
447 actomyosin arcs in their pSMAC (Fig. 7C1-C4, white arrows, and D).

448 Given these results, we asked if our PLB-engaged mouse GC B cells can
449 centralize antigen. In partial agreement with previous findings (61, 62), ~45% of
450 synapses exhibited small to medium sized antigen clusters distributed to varying
451 degrees in the synapse periphery (Fig. 7E1, E2 and F). In addition, ~20% of synapses
452 exhibited antigen microclusters spread throughout the synaptic interface (Fig. 7E3 and
453 F). Importantly, the remaining ~35% of synapses exhibited highly centralized antigen
454 (Fig. 7E4 and F). We conclude, therefore, that GC B cells can make actomyosin arcs
455 and centralize antigen like naïve B cells, although the degree to which they do these
456 two things is considerably less than for naïve B cells.

457

Discussion

Integrin co-stimulation promotes B cell activation and IS formation when antigen is limiting by promoting B cell adhesion (18, 19). Here we identified an actomyosin-dependent component of this integrin co-stimulatory effect. By combining super-resolution imaging with specific cytoskeletal perturbations, we showed that integrin ligation induces the formation of a pSMAC actomyosin arc network that comprises the major actin network at the primary B cell IS. This network is created by the formin mDia1, organized into a concentric, contractile structure by the molecular motor M2A, and promotes synapse formation by mechanically sweeping antigen clusters centripetally into the cSMAC. Most importantly, we showed that integrin-dependent synapse formation under conditions of limiting antigen requires M2A, as inhibiting its contractility significantly impairs antigen centralization. Consistently, myosin inhibition also diminishes the synaptic content of the key BCR signaling proteins P-CD79a and P-CD19 and disrupts their synaptic distribution. Finally, we showed that a significant fraction of GC B cells also make this contractile pSMAC actomyosin arc network. Together, our results argue that integrin co-stimulation promotes B cell activation and synapse formation not only by enhancing B cell adhesion (18), but also by eliciting the formation of a contractile actomyosin arc network that drives mechanical force-dependent IS formation. These findings invite a critical “reset” for the way in which future B cell studies should be approached by highlighting the need for integrin co-stimulation when examining the role of actin during B cell activation. This reset is especially important given that most *in vitro* studies of B cell IS formation and activation have been performed under conditions of excess antigen, while antigen is rarely available in excess *in vivo*.

A central player in the link between integrin co-stimulation and the formation of the actomyosin arc network is almost certainly active RhoA. First, active RhoA would drive arc formation by simultaneously targeting, unfolding and activating mDia1 at the plasma membrane (63, 64). Second, active RhoA would drive arc organization and contractility by activating the ROCK-dependent phosphorylation of the regulatory light chains on M2A (43), thereby promoting the assembly of the M2A bipolar filaments that decorate, organize and contract the arcs. Finally, it is likely that active RhoA would promote actomyosin arc formation by activating the ROCK-dependent phosphorylation of mDia1’s autoinhibitory domain, thereby blocking its refolding and subsequent inactivation (65-67). Given all this, it seems very likely that integrin ligation promotes actomyosin arc formation at least in part by promoting the loading of RhoA with GTP. Consistent with this idea, adhesion signaling has been linked in a variety of systems to the activation of guanine nucleotide exchange factors (GEFs) for RhoA (e.g. p190RhoGEF, GEF H1) (68, 69). Future work should seek, therefore, to clarify the outside-in signaling pathway in B cells that links integrin ligation to the activation of one

or more GEFs for RhoA. Such efforts should also take into account parallel activation pathways, such as the PI3K-dependent activation of RhoA downstream of BCR signaling (70), the myosin-dependent activation of B cell adhesion downstream of CXCR5 signaling (71), and the diacylglycerol kinase-dependent regulation of adhesion and actomyosin force generation at the B cell synapse (72). Given our results here, the ability of the B-cell integrin VLA-4, which binds VCAM-1 on APCs, to promote IS formation under limiting antigen conditions (19) may also involve an actomyosin-dependent mechanism. Indeed, actomyosin-dependent B cell IS formation may be a mechanism harnessed by multiple co-stimulatory pathways to promote B cell activation.

Consistent with our findings, a recent study by Bolger-Munro *et al.* reported that GFP-tagged M2A localizes to the medial portion of synapses formed by A20 B cells (13). In their hands, however, BB treatment did not inhibit antigen centralization, arguing that synapse formation does not require M2A. The disparity between their results and ours as regards the functional significance of M2A may be due to numerous differences in experimental design, including the cell type used (primary B cells versus the A20 B cell line), the mode of antigen presentation (anti-IgM-containing PLBs versus transmembrane antigen expressed by APCs), and the density of antigen (known in PLBs versus unknown and variable on APCs). Our pSMAC actomyosin arcs may also be related to the myosin-rich regions that form in primary HEL-specific naïve B cells bound to acrylamide gels coated with HEL antigen (47).

The contractile actomyosin structure identified here occupies the portion of the B-cell synapse defined by the presence of an integrin ring, i.e. the pSMAC (3, 18, 19, 73). This co-localization supports a feed-forward relationship where integrin co-stimulation promotes the formation of the actomyosin arcs, and the contractile forces that these arcs then exert promote further integrin activation and robust adhesion. Indeed, the B cell pSMAC can be viewed as roughly analogous to the lamellar region of mesenchymal cells, where integrins present within ECM-anchored focal adhesions are kept in their open, extended, high-affinity conformation by the forces that myosin-rich stress fibers exert on them (74, 75). By analogy, the contribution that the centering forces exerted by the actomyosin arcs make to integrin activation in the pSMAC may be enhanced in the context of an APC by the fact that the APC restricts ICAM-1 mobility (76).

Having established that naive B cells use actomyosin arcs to promote IS formation, an obvious next question is whether they also use this contractile structure to drive the extraction of membrane-bound antigens, a process known to require M2A (61, 77-79). Imaging synaptic actin and myosin in naïve B cells during the process of antigen extraction should shed considerable light on this question. In that vein, Roper *et al.* reported recently that the synapse of naïve B cells undergoing antigen extraction from antigen-bearing plasma membrane sheets (PMSs) is composed of a dynamic mixture of

Arp2/3 complex-dependent actin foci and formin-dependent linear filaments/fibers (80). While static images showed little co-localization between the actin foci and antigen clusters, dynamic imaging suggested that the foci promote antigen extraction (although the Arp2/3 complex and formins were both required for antigen uptake). Based on these and other observations, Roper *et al.* concluded that naive B cells use a foci-filament network to drive force-dependent antigen extraction (80). How M2A provides the force in this context was unclear, however, as M2A (visualized using an antibody to the phosphorylated form of M2A's RLC) did not co-localize with either actin structure. Moreover, neither actin structure was affected by BB treatment. Of note, these two findings are at odds with our findings here that M2A (visualized by endogenous tagging of the M2A heavy chain) co-localizes extensively with actin arcs, and that BB treatment profoundly disrupts the organization of the pSMAC actin arc network. Finally, we note that the images of synaptic actin presented by Roper *et al.* look similar to our images of naïve B cells stimulated with anti-IgM alone (i.e. without ICAM-1), where the synapse was also composed of a disorganized and dynamic mixture of actin foci and short actin filaments/fibers. The fact that the PMSs used by Roper *et al*. do not present any integrin ligands may explain, therefore, why they did not see a more organized synapse containing actomyosin arcs.

While the force-dependent extraction of antigens by naïve B cells commonly initiates the process of antibody production, the force-dependent extraction of antigens by GC B cells is thought to drive the subsequent process of antibody affinity maturation by selecting for BCR: antigen interactions of higher affinity (2, 81). Consistently, GC B cells possess higher levels of active M2A and exert stronger pulling forces than naive B cells, allowing them to extract antigens with higher affinities for the BCR (61, 62). Recent studies have shown that GC B cells accumulate antigen at the periphery of their synapse in association with actin-rich surface projections that mediate antigen extraction (61, 62). The striking difference between this behavior and that of naïve B cells, which centralize antigen prior to extraction, argues that GC B cells must differ dramatically from naïve B cells with regard to the organization of actomyosin at their synapse. We found, however, that about one third of GC B cells formed actomyosin arcs that were indistinguishable from those formed by naïve B cells. Moreover, about one third of GC B cells centralized antigen (although about half exhibited peripheral antigen clusters like those previously reported). While additional work is required to prove that the subset of GC B cells with actomyosin arcs are the ones that centralize antigen, this seems likely given our evidence here that actomyosin arcs drive antigen centralization in naïve B cells. Future work will also be required to understand why GC B cells vary with regard to actomyosin organization and the ability to centralize antigen (e.g. dark zone versus light zone GCs). That said, our results argue that the manner in which GC B cells harness actomyosin forces to extract antigen during the process of antibody affinity maturation may not be restricted to the previously reported pathway

(61, 62). Finally, we note that the PLBs and PMSs employed in those studies to image synaptic actin and antigen extraction did not contain integrin ligands. Given our results here, this might explain why the GC B cells in those studies did not contain actomyosin arcs.

Finally, future efforts should seek to define the role(s) played by the actomyosin arcs described here in the process of extracting membrane-bound antigen, as this process is impaired when M2A is inhibited or deleted (61, 77, 79). At a minimum, the ability of the actomyosin arcs to centralize and corral antigen at the cSMAC should promote antigen extraction no matter the exact extraction mechanism (15-17). As for a more direct role, the ability of the actomyosin arcs to create a ring of strong adhesion within the pSMAC that can grip the APC tightly may be required to extract antigens with high affinity for the BCR, much as a tight grip on the wine bottle is required to pull out its cork. This contractile structure also promotes both proximal signaling and the formation of larger antigen clusters, two processes that are likely linked mechanistically through the phase separation-dependent enhancement of signaling pathways (82). Whether the pSMAC actomyosin arcs contribute directly to the upward pulling forces inside the B cell that are thought to drive antigen extraction is, at the moment, unknown. Relevant to this question, M2A was not detected in the dispersed actin foci thought to mediate antigen extraction by naïve B cells engaged with antigen-bearing PMSs (80), or in the actin-rich, invadopodia-like structures thought to mediate antigen extraction by naïve B cells engaged with antigen-bearing acrylamide gels (47). Moreover, an association between M2A and the peripheral actin-rich pods thought to mediate antigen extraction by GC B cells engaged with antigen-bearing PMSs (62) has yet to be reported. We also note that none of the activating surfaces used in these studies contained integrin ligands, and that none of these studies examined antigen extraction in the context of a physiologically relevant form of antigen presentation (e.g. via Fc or complement receptors on the surface of a living cell). Given all this, further efforts to define the mechanism by which M2A powers the extraction of membrane-bound antigens should follow the myosin as the B cell extracts antigen from an APC, where the B cell's integrins will be engaged, and where the antigen can be presented in a physiologically relevant way. Perhaps only then will the role(s) played by M2A in antigen extraction be fully revealed.

Materials and Methods

Mice and cell culture

Primary B cells were isolated from the spleens of 6 to 12 week-old C57BL/6 mice (Jackson Laboratories #002595) and M2A-GFP KI mice (gift of R. Adelstein, NHLBI/NIH) of either sex using negative selection B cell isolation (StemCell Technologies). Euthanasia was performed in accordance with protocols approved by the National Human Genome Research Institute Animal Use and Care Committee at the National Institutes of Health. The A20 murine IgG^+ B cell line was from ATCC (ATCC® TIB-208™). B cells were cultured in complete medium (RPMI-1640, 10% heat-inactivated fetal calf serum (FCS), 2 mM L-glutamine, 1 mM sodium pyruvate, 50 µM 2-mercaptoethanol and 1X Antibiotic-Antimycotic) at 37 ^oC with 5% CO_2. Primary B cell complete media also contains 5 ng/ml of BAFF (R&D Systems).

Plasmids and Reagents

GFP- and tdTomato-tagged F-Tractin were gifts from Michael Schell (Uniformed Services University, Maryland). Alexa Fluor-conjugated phalloidins were purchased from Thermo Fisher. Anti-mDia1 antibody was purchased from Thermo Fisher (PA5-27607). HRP-conjugated mouse anti-β-actin antibody was purchased from Santa Cruz (SC-47778 HRP). Rabbit anti-CD79a (#3351), anti-PCD79a (#5173), anti-CD19 (#3574) and anti-PCD19 (#3571) were purchased from Cell Signaling Technologies. Anti-M2A was purchased from Millipore Sigma (#M8064) CK-666 and SMIFH2 were purchased from Millipore Sigma and used at final concentrations of 100 µM and 25 µM, respectively. pnBB and paBB were purchased from Cayman Chemicals and used at a final concentration of 25 µM. DMSO vehicle control was purchased from Millipore Sigma. CellMask™ Deep Red Plasma Membrane Stain was purchased from Thermo Fisher. Alexa Fluor 488- (#111-545-003), 594- (#111-585-003) and 647- (#111-605-003) conjugated goat, anti-rabbit secondary antibodies were purchased from Jackson ImmunoResearch. Goat anti-mouse IgG Fcγ fragment specific antibody (#115-005-008) and goat anti-mouse IgM, µ-chain specific antibodies (#115-005-020) were purchased from Jackson ImmunoResearch. Anti-rabbit-HRP (#32260) was purchased from Thermo Fisher.

GC B cell generation and sorting

GC B cells were generated and sorted using a previously described protocol (83). Briefly, 6 to 12 week-old M2A-GFP KI mice were immunized with sheep's red blood cells. After 8 to 10 days, total B cells from the spleens and lymph nodes were isolated using the Negative Selection B cell isolation kit (Stemcell Technologies) according to the manufacturer's instructions. Dead cells were stained using Zombie Yellow viability stain (Biolegend) and Fc receptors were blocked with the mouse TruStain FcX™ antibody (#156604). Cells were immunostained with anti-mouse CD38 (#102719), B220

(#103235) and GL-7 (#144617) purchased from Biolegend. GC B cells were sorted on a BD Aria III FACs sorter (Beckton Dickinson) for GFP+, Zombie Yellow^{-}, B220^{+}, CD38^{low} and GL-7^{+} cells, and were used immediately.

B cell transfection

A20 B cells and primary B cells were transfected as previously described (25). Briefly, e*x vivo* primary B cells were first cultured for 12 h in complete media supplemented with 5 ng/ml BAFF (R&D Systems) and 2.5 µg/ml *Escherichia coli* O111:B4 LPS (Millipore Sigma) (LPS was included to promote cell survival during nucleofection). 2x10^{6} B cells were then nucleofected with 2 µg of plasmid DNA using Nucleofector Kit V (Lonza) and rested for 16-24 hours using complete media containing 5 ng/ml BAFF and lacking LPS. We refer to both rested, transfected cells and *ex vivo* non-manipulated cells as naïve B cells because neither had been activated by antigen.

CRISPR

Mouse GFP-M2A and Scarleti-M2A template plasmids were gifts from Jordan Beach (Loyola University, Chicago). Mouse M2A sgRNAs were synthesized by Synthego and used according to the manufacturer's instructions. Briefly, sgRNAs were mixed with Cas9 (New England Biolabs) to form ribonucleoproteins and then added together with 0.5 µg of template plasmid to 2x10^{6} cells suspended in the solution for Nucleofector kit V. Following nucleofection, the cells were cultured in complete media for 24 hours before Fluorescence-activated cell sorting (FACS) for GFP or Scarleti expression using the Aria III (Becton Dickinson).

miRNA-mediated knockdown of mDia1

miRNAs targeting the 3' UTR of mouse mDia1 were designed as previously described (84) using BLOCK-iT RNAi Designer (Thermo Fisher), synthesized (Gene Universal), and fused to the C-terminus of mNeonGreen-F-Tractin using In-Fusion cloning (Takara). A20 B cells were transfected with 2 µg of F-Tractin-mNeonGreen vector control or F-Tractin-mNeonGreen-mDia1-miRNAs and cultured in complete media for 16 hrs. Cells were then lysed and immunoblotted using an antibody to DIAPH1 (1:250; Thermo Fisher, PA5-27607) and an HRP-conjugated antibody to β-actin (1:5000; Santa Cruz, SC-47778 HRP) to confirm knockdown. Cells that had received the miRNA were identified based on the expression of F-Tractin-mNeonGreen and then quantified. F-Tractin-mNeonGreen-positive cells were also used in a cell spreading assay as described above. See Supplementary information for additional details.

Cell spreading on functionalized glass

8-well Labtek chambers (Nunc) were coated with 15 µg/ml of anti-IgM and/or anti-IgG with or without 0.5 µg/ml of mouse histidine-tagged ICAM-1 (Sino Biological) for 1 hour

at room temperature. B cells were resuspended in modified HEPES-buffered saline (mHBS) (25) and adhered to functionalized glass for 15 min at 37°C before live-imaging or fixing with 4% paraformaldehyde for staining (see SI Materials and Methods). Where inhibitors were used, cells were pretreated for 30 min with 100 µM CK-666, 25 µM SMIFH2, 25 µM pnBB or paBB, or dH_2O/DMSO vehicle control in mHBS at 37 ^oC. Cells were then added to functionalized Labtek chambers in mHBS containing the same concentrations of inhibitors or vehicle control as the pretreatment.

Supported planar lipid bilayers

Liposomes were prepared as described previously (26, 27, 85). Briefly, 0.4mM 1,2-dioleoyl-*sn*-glycero-3-phosphocholine, biotin–CAP-PE, 1,2-dioleoyl-*sn*-glycero-3-[(*N*-(5-amino-1-carboxypentyl)iminodiacetic acid)succinyl] (DGS)–NTA and 1,2-dioleoyl-sn-glycero-3-phosphocholine (Avanti Polar Lipids, Inc.) were mixed at 1:3:96 molar % ratio. Lipids were dried under a stream of argon and then desiccated in a vacuum chamber. Unilamellar liposomes were generated from lyophilized lipids hydrated in Tris-buffered saline via extrusion through a 50-nm pore membrane using a mini-extruder kit (Avanti Polar Lipids, Inc.). PLBs were assembled in Sticky-Slide VI$^{0.4}$ Luer closed chambers (Ibidi) as previously described (86). 25 × 75-mm glass coverslips (Ibidi) were cleaned using Piranha solution (1:3 ratio of sulfuric acid and 30% hydrogen peroxide). After depositing liposomes onto the flow channels, the channels were washed with HBS buffer containing 1% BSA. A solution containing mono-biotinylated, Alexa Fluor 647-labeled anti-IgM antibody (0.15 µg/ml for the limiting antigen condition and 2 µg/ml for the high antigen condition) and streptavidin (Sigma-Aldrich) were added to the flow chambers with or without 0.5 µg/ml unlabeled histidine-tagged ICAM-1. Anti-IgM antibody (µ-chain specific) was monobiotinylated and labeled with Alexa Fluor 647 (Thermo Fisher) as described previously (18). The uniformity and lateral mobility of PLBs were assessed using FRAP as described previously (26). Photo bleached spots typically recovered within 60 seconds). B cells were resuspended in modified HEPES-buffered saline and allowed to engage PLBs at 37°C and imaged immediately, or fixed with 4% paraformaldehyde after 5 and 10 mins for immunostaining.

Traction force microscopy

Polyacrylamide gels (PA, 0.23 kPa shear modulus, 40 µm thickness) were prepared on glass coverslips with embedded 40 nm fluorescent beads (TransFluoSpheres (633/720), Thermo Scientific), as described previously (87). B cells were resuspended in mHBS with 2% FCS and added to PA gels. Images of B cells that had engaged PA gels for 20 mins were captured. A no-stress reference image of the PA gels with beads was captured after lifting cells from the PA gel by adding 1% sodium dodecyl sulfate in 1X PBS to the imaging chamber at a final concentration of 0.04%. Particle image velocimetry was used to calculate bead displacements relative to the reference position,

and the corresponding contractile energy was quantified using ImageJ plugins as previously described (87, 88). Traction forces were reported as the mean magnitude of traction stress within the cell relative to the cell surface area.

Immunostaining

Fixed cells were permeabilized with 0.2% Triton-X-100 and blocked for 30 min at room temperature using PBS containing 2% BSA. Cells were incubated with primary antibodies (1:200) overnight at 4°C and then secondary antibodies (1:250) with Alexa Fluor-conjugated phalloidins for 1h at room temperature. Antibodies and phalloidins were diluted in blocking buffer. All washes were performed with 1X PBS.

Microscopy

All live cell imaging was performed at 37 °C in mHBS supplemented with 2% FCS. TIRF-SIM and 3D-SIM imaging were performed on a GE DeltaVision OMX SR microscope (Cytiva) equipped with a 60X 1.42 NA oil objective (Olympus). For 3D-SIM, *z*-stacks were acquired at 0.125 µm increments. Raw data were reconstructed using Softworx software (Cytiva) with a Wiener filter constant of 0.002-0.003. Airyscan imaging was performed using an LSM 880 Zeiss confocal microscope equipped with Airyscan and using a Plan-Apochromat 63X 1.4 NA oil objective. Airyscan image reconstruction was performed using Zeiss ZEN imaging software. TFM was imaged using a Nikon Eclipse Ti2 microscope equipped with a 60X 1.2 NA water objective. Linear adjustments to images were made using ImageJ 1.53 (NIH).

Image analyses

All image analysis was performed using ImageJ (NIH). To compare the relative fraction of total IS footprint occupied by the cSMAC, pSMAC and dSMAC, the SMAC areas were manually drawn based on actin morphology (dendritic for dSMAC, actin arc for pSMAC, and hypodense for cSMAC) and then compared to the total IS area, which was determined based on thresholds for F-actin intensity at the synaptic interface. Fluorescence intensity within the SMAC regions was quantified using the ROIs from above and reported as the total background-corrected fluorescence within the ROI, which was quantified as described (89) using the following equation: Integrated density–[(area of ROI)×(mean background fluorescence per unit area)], where the integrated density is equal to [(area of ROI)×(mean fluorescence per unit area within the ROI)]. Mean background fluorescence was determined using the same ROI size at 3 separate positions less than 3 µm away from the cell. The myosin fluorescence intensity in 3D SIM images was quantified using a maximum projection image of the image stacks where the cell ROI was determined based on the F-actin threshold and the background-corrected myosin fluorescence within the cell ROI was reported. The FibrilTool plugin for ImageJ was used to measure actin arc morphology as described previously (27, 45).

Briefly, the pSMAC regions in TIRF-SIM images were divided into 10-12 trapezoid-shaped ROIs of similar size to measure the anisotropy of arcs in the radially symmetric pSMAC. The values obtained range from 0, when the orientation of the structures is random, to 1, when the structures show higher orientation in the same direction. The velocity of centripetal actin flow was assessed by assembling kymographs from TIRF-SIM videos using the Kymograph Builder plugin from ImageJ, as previously described (27). Briefly, the dSMAC and pSMAC regions were identified by the relatively abrupt slope change for F-actin flow, and slope angles were used to quantify the rates of actin movement. The size of each antigen cluster and their relative distance from the cSMAC center were quantified using an ImageJ macro. First, the perimeter of the synaptic interface was determined based on thresholds for F-actin, and an ROI that encompassed the interface area was drawn (the synaptic ROI). The coordinates for each pixel contained in the ROI was determined and the linear distance of each pixel from the center of mass of the total synaptic antigen (defined as cSMAC center) was determined. The longest distance was defined as the furthest distance to travel from the outermost edge of the cell. A binary image of the antigen channel combined with the ImageJ watershed algorithm was used to segment individual antigen clusters within the synaptic ROI. The area of each antigen cluster was quantified using the Analyze Particles function in ImageJ. The relative distance of each antigen cluster was reported as the distance between the center of mass of the antigen cluster and the cSMAC center after normalizing to the furthest distance from the cell edge to the cSMAC center. To quantify the antigen fluorescence in the cSMAC, a circular ROI corresponding to 20% of the total synaptic area (based on the average area of the cSMAC at the synaptic interface) was drawn such that the center of the circle lies at the same coordinates as the center of mass of the total antigen signal Antigen fluorescence within this circle was quantified and presented as a percent of the total synaptic antigen fluorescence. The fluorescence intensity of the signaling molecules CD79a, P-CD79a, CD19 and P-CD19 were all reported as the total fluorescence intensity within the synaptic ROI. All fluorescence intensities were corrected for background as described above. Fluorescence intensity profiles were obtained by drawing a 10 μm line across the center of the synaptic interface and using the ImageJ function “Plot Profiles” to obtain fluorescence intensity values across the line. The intensity profiles of several cells were combined and the average fluorescence intensity ± standard deviation was reported. The speeds of antigen cluster movement were quantified using the ImageJ plugin TrackMate as previously described (90) where a combination of automated and manual tracking were performed. Prior to quantification, the perimeter of the cell was identified by over-saturating the signal for GFP-M2A, and the anti-IgM fluorescence signal outside of the cell was removed so that only antigen clusters formed by that cell were quantified. Antigen clusters were determined using a blob diameter of 0.2 μm^2 and tracks were obtained using a threshold of 2000 units with sub-pixel localization. Mean antigen

808 cluster movement speeds were reported as distance traveled over time. Kymographs of
809 moving antigen clusters were created using the ImageJ plugin Kymograph Builder.
810
811 **Statistical analyses**
812 All statistical analyses were performed using Prism 9 (GraphPad). Statistical
813 comparisons of dot plots were performed using unpaired, two-tailed *t*-tests, and data are
814 represented as mean ± standard deviation. Statistical comparisons of bar charts were
815 performed using paired, two-tailed *t*-tests, and data are represented as mean ±
816 standard error of the mean. The following annotations are used to indicate significance:
817 * = P<0.05, ** = P<0.01, *** = P<0.001, and **** = P<0.0001.
818

Acknowledgments

This work was supported by the Intramural Research Program of the National Heart, Lung, and Blood Institute (NHLBI) (1ZIAHL006121-04 to JAH). The authors thank the NHLBI Flow Cytometry Core, Dr. Xuefei Ma for providing M2A-GFP mice, Dr. Il-Young Hwang for immunizing mice to prepare GC B cells, and Dr. Christopher J. Alexander for advice on miRNA design.

Competing interests

We have no competing interests to disclose.

Figures

Figure 1. ICAM-1 co-stimulation promotes the formation of actin arcs at the B cell IS.

(A-F) GFP-F-Tractin-expressing primary B cells on glass coated with anti-IgM alone (A, B, E1, E2) or with anti-IgM+ICAM-1 (C, D, F1, F2) and imaged using Airyscan (A, C) or TIRF-SIM (B, D, E1, E2, F1, F2). The white arrows in A and B indicate the thin outer rim of dendritic actin in the dSMAC. The blue bars in A-D indicate the pSMAC. E2 and F2 correspond to the boxed regions in E1 and F1, respectively. (G) Percent of cells with pSMAC actin arcs (N>67 cells/condition from 3 experiments). (H, I) Percent of total synaptic F-actin (H) and percent of total IS footprint (I) contained within the dSMAC, pSMAC and cSMAC portions of the synapse for primary B cells on anti-IgG/ICAM-1-coated glass (N=44 cells/condition from 6 experiments). (J1, J2) GFP-F-Tractin-expressing A20 B cell on anti-IgG/ICAM-1-coated glass. J2 corresponds to the boxed region in J1. The red arrows in C, D and J1 indicate actin arcs. Scale bars: 10 µm.

Figure 2. The actin arcs are created by the formin mDia1 acting at the outer edge of the IS.

(A) GFP-F-Tractin-expressing primary B cell on anti-IgG/ICAM-1-coated glass. (B1, B2) Boxed regions in (A). (C1, C2) B1 and B2 with red lines applied to highlight linear actin filaments/bundles arising from surface spikes at the IS edge that are contiguous with actin arcs in the pSMAC. (D1, D2) GFP-F-Tractin-expressing primary B cell on anti-IgG/ICAM-1-coated glass before (D1) and 6 minutes after SMIFH2 addition (D2). (E) F-actin intensity profiles corresponding to the line scans in D1 (blue, before SMIFH2 addition) and D2 (red, after SMIFH2 addition). (F1-F4) GFP-F-Tractin-expressing A20 B cells transfected with vector-only or the indicated mDia1 miRNA constructs and activated on anti-IgG/ICAM-1-coated glass. (G) Ratio of pSMAC to dSMAC F-actin (N>20 cells/condition from 2 experiments). (H) pSMAC F-actin content (N=20-26 cells/condition from 2 experiments). A-C, and F: TIRF-SIM images; D: Airyscan images. Scale bars: 5 µm in A, D2, and F1; 2 µm in B1.

Figure 3. Myosin 2A decorates the actin arcs and is required for their concentric organization.

(A1-A5) Td-Tomato-F-Tractin expressing primary B cell from the M2A-GFP knockin mouse on anti-IgM/ICAM-1-coated glass. A4 and A5 correspond to the boxed regions in A1 and A2, respectively. (B1-B6) Still images at the indicated time points taken from a region within Movie 7 of a Td-Tomato-F-Tractin expressing primary B cell from the M2A-GFP knockin mouse. Different color arrowheads mark the formation and centripetal movement of individual M2A bipolar filaments (see text for details). (C, D) Phalloidin-

stained primary B cell from the M2A-GFP knockin mouse on glass coated with anti-IgM alone (C) or with anti-IgM+ICAM-1 (D). (E) Total synaptic M2A content (N=91-115 cells/condition from 3 experiments). (F, G) GFP-F-Tractin-expressing primary B cells that had been pretreated with DMSO (F) or pnBB (G) for 30 minutes and activated on anti-IgM/ICAM-1-coated glass. (H) Anisotropy of the actin filaments/bundles present within the pSMAC (see also Fig. S2H) (N=369-423 ROIs from 30-37 cells from 3 experiments). All panels: TIRF-SIM images. Scale bars: 3 µm in A3 and B6; 250 nm in A5; 5 µm in D and G.

Figure 4. Actin arcs sweep antigen clusters centripetally.

(A1-A3) Phalloidin-stained (green) primary B cell 15 min after engagement with a PLB containing unlabeled ICAM-1 and limiting anti-IgM (red). The white arrows in A1 and A3 mark the actin arcs. (B) Tracks of single anti-IgM microclusters traveling centripetally across the dSMAC (red tracks) and pSMAC (green tracks) acquired from Movie 9. The white line indicates the outer edge of this cell. (C) Mean speed of single anti-IgM microclusters moving centripetally across the dSMAC and pSMAC (N=180-273 tracks from 3 well-spread cells). (D1-D6) Still images at the indicated time points from Movie 10 showing the centripetal movement of actin arcs and a representative anti-IgM microcluster (white arrows) (the center of the synapse is directly below the images). Transparent white lines highlight the actin arcs that moved the microcluster centripetally. (E1-E6) Same as D1-D6 except showing only the anti-IgM microcluster, and indicating its centripetal path in blue. (F) Temporally pseudo-colored, projected image of the anti-IgM microcluster in (D) and (E). (G) Kymograph of the 3 µm-long paths taken by the microcluster and the actin arcs in (D) and (E) over a period of 400s. The white brackets on the right indicate where actin arcs overlapped with and moved the microcluster, while the red brackets indicate where the movement of the microcluster stalled. A: Airyscan images; D-G: TIRF-SIM images. Scale bars: 5 µm in A3 and B; 300 nm in D6 and F.

Figure 5. Integrin ligation-dependent IS formation requires myosin 2A contractility.

(A1-A3) DMSO-treated, phalloidin-stained primary B cells 15 min after engagement with a PLB containing ICAM-1 and limiting anti-IgM. (B1-B3) Same as A1-A3 except the B cells were treated with pnBB. (C1-C3) Images of a representative, DMSO-treated primary B cell (white arrows mark actin arcs). (D1-D3) Images of a representative, pnBB-treated primary B cell. (E) Percent of cells exhibiting centralized, partially centralized and non-centralized antigen (see Figure S5D1-D3 for representative examples of these three types of antigen distribution) (N=126-144 cells/condition from 3 experiments). (F) Percent of total synaptic antigen in the cSMAC (N=81-86 cells/condition from 3 experiments). (G) Antigen cluster size as a function of normalized

905 distance from the cSMAC center (N=113-144 cells/condition from 3 experiments). (H)
906 Total synaptic antigen content (N=56-62 cells/condition from 3 experiments). All panels:
907 Airyscan images. Scale bars: 10 µm in A1, B1, A3, and B3; 5 µm in D3.

908 **Figure 6. Myosin 2A contractility promotes BCR signaling.**

909 (A1-A4) DMSO-treated primary B cell 10 min after engagement with a PLB containing
910 ICAM-1 and limiting anti-IgM, and stained for F-actin and P-CD79a. (B1-B4) Same as
911 A1-A4 except the B cell was treated with pnBB. (C) Synaptic P-CD79a content (N=55-
912 81 cells/condition from 3 experiments). (D1-D4) DMSO-treated primary B cell 10 min
913 after engagement with a PLB containing ICAM-1 and limiting anti-IgM, and stained for
914 F-actin and P-CD19. (E1-E4) Same as D1-D4 except the cell was treated with pnBB. (F)
915 Synaptic P-CD19 content (N=115-140 cells/condition from 3 experiments). (G)
916 Fluorescence intensities across synapses for P-CD19 (red), antigen (grey), and F-actin
917 (green) in B cells treated with DMSO (N=22 cells from 2 experiments). The position of
918 the pSMAC is highlighted in blue. (H) Same as G except the cells were treated with
919 pnBB (N=16 cells from 2 experiments). All panels: Airyscan images. Scale bars: 5 µm in
920 B4; 3 µm in E4.

921 **Figure 7. GC B cells make actomyosin arcs.**

922 (A1-A3) Phalloidin-stained primary GC B cell from the M2A-GFP knockin mouse on anti-
923 IgM/anti-IgG/ICAM-1-coated glass. White arrows mark the actomyosin arcs. (B) Percent
924 of cells on glass that did or did not show M2A enrichment in the pSMAC (N=140 cells
925 from 4 experiments). (C) Phalloidin-stained primary GC B cell from the M2A-GFP
926 knockin mouse 15 min after engagement with a PLB containing anti-IgM, anti-IgG, and
927 ICAM-1. (D) Percent of cells on PLBs that did or did not show M2A enrichment in the
928 pSMAC (N=89 cells from 4 experiments). (E1-E4) Representative images of the three
929 types of anti-Ig distribution exhibited by GC B cells 15 min after engagement with a PLB
930 containing anti-IgG and ICAM-1 (cell outlines are shown in blue). (F) Percent of GC
931 cells displaying the three types of anti-Ig distribution shown in E1-E4 (N=157 cells from
932 6 experiments). All panels: TIRF-SIM images. Scale bars: 5 µm in A3; 3 µm in C4 and
933 E4.

934

935

936

References

1. Forthal DN, Functions of Antibodies. *Microbiol. Spectr.* **2,** 1-17 (2014).
2. Heesters BA, van der Poel CE, Das A, & Carroll MC, Antigen Presentation to B Cells. *Trends in Immunology* **37,** 844-854 (2016). 10.1016/j.it.2016.10.003.
3. Harwood NE & Batista FD, The cytoskeleton coordinates the early events of B-cell activation. *Cold Spring Harb. Perspect. Biol.* **3,** a002360 (2011). 10.1101/cshperspect.a002360.
4. Gonzalez SF*, et al.*, Trafficking of B cell antigen in lymph nodes. *Annu. Rev. Immunol.* **29,** 215-233 (2011). 10.1146/annurev-immunol-031210-101255.
5. Carrasco YR & Batista FD, B cell recognition of membrane-bound antigen: an exquisite way of sensing ligands. *Curr. Opin. Immunol.* **18,** 286-291 (2006). 10.1016/j.coi.2006.03.013.
6. Cyster JG, B cell follicles and antigen encounters of the third kind. *Nat. Immunol.* **11,** 989-996 (2010). 10.1038/ni.1946.
7. Wang JC & Hammer JA, The role of actin and myosin in antigen extraction by B lymphocytes. *Semin. Cell Dev. Biol.* **102,** 90-104 (2020). 10.1016/j.semcdb.2019.10.017.
8. Song W, Liu C, & Upadhyaya A, The pivotal position of the actin cytoskeleton in the initiation and regulation of B cell receptor activation. *Biochim. Biophys. Acta* **1838,** 569-578 (2014). 10.1016/j.bbamem.2013.07.016.
9. Fleire SJ*, et al.*, B cell ligand discrimination through a spreading and contraction response. *Science* **312,** 738-741 (2006). 10.1126/science.1123940.
10. Tolar P, Sohn HW, Liu W, & Pierce SK, The molecular assembly and organization of signaling active B-cell receptor oligomers. *Immunol. Rev.* **232,** 34-41 (2009). 10.1111/j.1600-065X.2009.00833.x.
11. Mattila PK, Batista FD, & Treanor B, Dynamics of the actin cytoskeleton mediates receptor cross talk: An emerging concept in tuning receptor signaling. *J. Cell Biol.* **212,** 267-280 (2016). 10.1083/jcb.201504137.
12. Treanor B, Harwood NE, & Batista FD, Microsignalosomes: spatially resolved receptor signalling. *Biochem. Soc. Trans.* **37,** 1014-1018 (2009). 10.1042/BST0371014.
13. Bolger-Munro M*, et al.*, Arp2/3 complex-driven spatial patterning of the BCR enhances immune synapse formation, BCR signaling and cell activation. *Elife* **8,** (2019). 10.7554/eLife.44574.
14. Batista FD, Treanor B, & Harwood NE, Visualizing a role for the actin cytoskeleton in the regulation of B-cell activation. *Immunol. Rev.* **237,** 191-204 (2010). 10.1111/j.1600-065X.2010.00943.x.
15. Batista FD, Iber D, & Neuberger MS, B cells acquire antigen from target cells after synapse formation. *Nature* **411,** 489-494 (2001). 10.1038/35078099.
16. Yuseff MI, Pierobon P, Reversat A, & Lennon-Dumenil AM, How B cells capture, process and present antigens: a crucial role for cell polarity. *Nat. Rev. Immunol.* **13,** 475-486 (2013). 10.1038/nri3469.
17. Yuseff MI & Lennon-Dumenil AM, B cells use conserved polarity cues to regulate their antigen processing and presentation functions. *Front. Immunol.* **6,** 251 (2015). 10.3389/fimmu.2015.00251.
18. Carrasco YR, Fleire SJ, Cameron T, Dustin ML, & Batista FD, LFA-1/ICAM-1 interaction lowers the threshold of B cell activation by facilitating B cell adhesion and synapse formation. *Immunity* **20,** 589-599 (2004).
19. Carrasco YR & Batista FD, B-cell activation by membrane-bound antigens is facilitated by the interaction of VLA-4 with VCAM-1. *EMBO J.* **25,** 889-899 (2006). 10.1038/sj.emboj.7600944.

20. Springer TA, Adhesion receptors of the immune system. *Nature* **346,** 425-434 (1990). 10.1038/346425a0.
21. Springer TA, Dustin ML, Kishimoto TK, & Marlin SD, The lymphocyte function-associated LFA-1, CD2, and LFA-3 molecules: cell adhesion receptors of the immune system. *Annu. Rev. Immunol.* **5,** 223-252 (1987). 10.1146/annurev.iy.05.040187.001255.
22. Wang JC, Bolger-Munro M, & Gold MR, Visualizing the Actin and Microtubule Cytoskeletons at the B-cell Immune Synapse Using Stimulated Emission Depletion (STED) Microscopy. *J. Vis. Exp.* (2018). 10.3791/57028.
23. Freeman SA*, et al.*, Cofilin-mediated F-actin severing is regulated by the Rap GTPase and controls the cytoskeletal dynamics that drive lymphocyte spreading and BCR microcluster formation. *J. Immunol.* **187,** 5887-5900 (2011). 10.4049/jimmunol.1102233.
24. Liu C*, et al.*, Actin reorganization is required for the formation of polarized B cell receptor signalosomes in response to both soluble and membrane-associated antigens. *J. Immunol.* **188,** 3237-3246 (2012). 10.4049/jimmunol.1103065.
25. Wang JC*, et al.*, The Rap1-cofilin-1 pathway coordinates actin reorganization and MTOC polarization at the B cell immune synapse. *J. Cell Sci.* **130,** 1094-1109 (2017). 10.1242/jcs.191858.
26. Yi J, Wu XS, Crites T, & Hammer JA, 3rd, Actin retrograde flow and actomyosin II arc contraction drive receptor cluster dynamics at the immunological synapse in Jurkat T cells. *Mol. Biol. Cell* **23,** 834-852 (2012). 10.1091/mbc.E11-08-0731.
27. Murugesan S*, et al.*, Formin-generated actomyosin arcs propel T cell receptor microcluster movement at the immune synapse. *J. Cell Biol.* **215,** 383-399 (2016). 10.1083/jcb.201603080.
28. Goode BL & Eck MJ, Mechanism and function of formins in the control of actin assembly. *Annu. Rev. Biochem.* **76,** 593-627 (2007). 10.1146/annurev.biochem.75.103004.142647.
29. Breitsprecher D & Goode BL, Formins at a glance. *J. Cell Sci.* **126,** 1-7 (2013). 10.1242/jcs.107250.
30. Chen Q, Nag S, & Pollard TD, Formins filter modified actin subunits during processive elongation. *J. Struct. Biol.* **177,** 32-39 (2012). 10.1016/j.jsb.2011.10.005.
31. Rizvi SA*, et al.*, Identification and characterization of a small molecule inhibitor of formin-mediated actin assembly. *Chem. Biol.* **16,** 1158-1168 (2009). 10.1016/j.chembiol.2009.10.006.
32. Nishimura Y*, et al.*, The formin inhibitor SMIFH2 inhibits members of the myosin superfamily. *J. Cell Sci.* **134,** (2021). 10.1242/jcs.253708.
33. Burke TA*, et al.*, Homeostatic actin cytoskeleton networks are regulated by assembly factor competition for monomers. *Curr. Biol.* **24,** 579-585 (2014). 10.1016/j.cub.2014.01.072.
34. Lomakin AJ*, et al.*, Competition for actin between two distinct F-actin networks defines a bistable switch for cell polarization. *Nat. Cell Biol.* **17,** 1435-1445 (2015). 10.1038/ncb3246.
35. Fritzsche M, Erlenkamper C, Moeendarbary E, Charras G, & Kruse K, Actin kinetics shapes cortical network structure and mechanics. *Sci. Adv.* **2,** e1501337 (2016). 10.1126/sciadv.1501337.
36. Hammer JA, Wang JC, Saeed M, & Pedrosa AT, Origin, Organization, Dynamics, and Function of Actin and Actomyosin Networks at the T Cell Immunological Synapse. *Annu. Rev. Immunol.* **37,** 201-224 (2019). 10.1146/annurev-immunol-042718-041341.
37. Vicente-Manzanares M, Ma X, Adelstein RS, & Horwitz AR, Non-muscle myosin II takes centre stage in cell adhesion and migration. *Nat. Rev. Mol. Cell Biol.* **10,** 778-790 (2009). 10.1038/nrm2786.
38. Sellers JR, Myosins: a diverse superfamily. *Biochim. Biophys. Acta* **1496,** 3-22 (2000). 10.1016/s0167-4889(00)00005-7.
39. Shutova MS & Svitkina TM, Common and Specific Functions of Nonmuscle Myosin II Paralogs in Cells. *Biochemistry (Mosc)* **83,** 1459-1468 (2018). 10.1134/S0006297918120040.

40. Zhang Y, *et al.*, Mouse models of MYH9-related disease: mutations in nonmuscle myosin II-A. *Blood* **119,** 238-250 (2012). 10.1182/blood-2011-06-358853.
41. Beach JR, *et al.*, Nonmuscle myosin II isoforms coassemble in living cells. *Curr. Biol.* **24,** 1160-1166 (2014). 10.1016/j.cub.2014.03.071.
42. Beach JR, *et al.*, Actin dynamics and competition for myosin monomer govern the sequential amplification of myosin filaments. *Nat. Cell Biol.* **19,** 85-93 (2017). 10.1038/ncb3463.
43. Beach JR & Hammer JA, 3rd, Myosin II isoform co-assembly and differential regulation in mammalian systems. *Exp. Cell Res.* **334,** 2-9 (2015). 10.1016/j.yexcr.2015.01.012.
44. Kepiro M, *et al.*, para-Nitroblebbistatin, the non-cytotoxic and photostable myosin II inhibitor. *Angew. Chem. Int. Ed. Engl.* **53,** 8211-8215 (2014). 10.1002/anie.201403540.
45. Boudaoud A, *et al.*, FibrilTool, an ImageJ plug-in to quantify fibrillar structures in raw microscopy images. *Nat. Protoc.* **9,** 457-463 (2014). 10.1038/nprot.2014.024.
46. Wang J, *et al.*, Profiling the origin, dynamics, and function of traction force in B cell activation. *Sci. Signal.* **11,** (2018). 10.1126/scisignal.aai9192.
47. Kumari A, *et al.*, Actomyosin-driven force patterning controls endocytosis at the immune synapse. *Nat. Commun.* **10,** 2870 (2019). 10.1038/s41467-019-10751-7.
48. Gardel ML, Schneider IC, Aratyn-Schaus Y, & Waterman CM, Mechanical integration of actin and adhesion dynamics in cell migration. *Annu. Rev. Cell. Dev. Biol.* **26,** 315-333 (2010). 10.1146/annurev.cellbio.011209.122036.
49. Case LB & Waterman CM, Integration of actin dynamics and cell adhesion by a three-dimensional, mechanosensitive molecular clutch. *Nat. Cell Biol.* **17,** 955-963 (2015). 10.1038/ncb3191.
50. Comrie WA & Burkhardt JK, Action and Traction: Cytoskeletal Control of Receptor Triggering at the Immunological Synapse. *Front. Immunol.* **7,** 68 (2016). 10.3389/fimmu.2016.00068.
51. Schnyder T, *et al.*, B cell receptor-mediated antigen gathering requires ubiquitin ligase Cbl and adaptors Grb2 and Dok-3 to recruit dynein to the signaling microcluster. *Immunity* **34,** 905-918 (2011). 10.1016/j.immuni.2011.06.001.
52. Hashimoto-Tane A, *et al.*, Dynein-driven transport of T cell receptor microclusters regulates immune synapse formation and T cell activation. *Immunity* **34,** 919-931 (2011). 10.1016/j.immuni.2011.05.012.
53. Yu CH, Wu HJ, Kaizuka Y, Vale RD, & Groves JT, Altered actin centripetal retrograde flow in physically restricted immunological synapses. *PLoS One* **5,** e11878 (2010). 10.1371/journal.pone.0011878.
54. Ditlev JA, *et al.*, A composition-dependent molecular clutch between T cell signaling condensates and actin. *Elife* **8,** (2019). 10.7554/eLife.42695.
55. Smoligovets AA, Smith AW, Wu HJ, Petit RS, & Groves JT, Characterization of dynamic actin associations with T-cell receptor microclusters in primary T cells. *J. Cell Sci.* **125,** 735-742 (2012). 10.1242/jcs.092825.
56. Varkuti BH, *et al.*, A highly soluble, non-phototoxic, non-fluorescent blebbistatin derivative. *Sci. Rep.* **6,** 26141 (2016). 10.1038/srep26141.
57. Tanaka S & Baba Y, B Cell Receptor Signaling. *Adv. Exp. Med. Biol.* **1254,** 23-36 (2020). 10.1007/978-981-15-3532-1_2.
58. Tuveson DA, Carter RH, Soltoff SP, & Fearon DT, CD19 of B cells as a surrogate kinase insert region to bind phosphatidylinositol 3-kinase. *Science* **260,** 986-989 (1993). 10.1126/science.7684160.
59. Keppler SJ, *et al.*, Wiskott-Aldrich Syndrome Interacting Protein Deficiency Uncovers the Role of the Co-receptor CD19 as a Generic Hub for PI3 Kinase Signaling in B Cells. *Immunity* **43,** 660-673 (2015). 10.1016/j.immuni.2015.09.004.

60. Depoil D*, et al.*, CD19 is essential for B cell activation by promoting B cell receptor-antigen microcluster formation in response to membrane-bound ligand. *Nat. Immunol.* **9,** 63-72 (2008). 10.1038/ni1547.
61. Nowosad CR, Spillane KM, & Tolar P, Germinal center B cells recognize antigen through a specialized immune synapse architecture. *Nat. Immunol.* **17,** 870-877 (2016). 10.1038/ni.3458.
62. Kwak K*, et al.*, Intrinsic properties of human germinal center B cells set antigen affinity thresholds. *Sci. Immunol.* **3,** (2018). 10.1126/sciimmunol.aau6598.
63. Kuhn S & Geyer M, Formins as effector proteins of Rho GTPases. *Small GTPases* **5,** e29513 (2014). 10.4161/sgtp.29513.
64. Rose R*, et al.*, Structural and mechanistic insights into the interaction between Rho and mammalian Dia. *Nature* **435,** 513-518 (2005). 10.1038/nature03604.
65. Nezami AG, Poy F, & Eck MJ, Structure of the autoinhibitory switch in formin mDia1. *Structure* **14,** 257-263 (2006). 10.1016/j.str.2005.12.003.
66. Maiti S*, et al.*, Structure and activity of full-length formin mDia1. *Cytoskeleton (Hoboken, N.J.)* **69,** 393-405 (2012). 10.1002/cm.21033.
67. Staus DP, Taylor JM, & Mack CP, Enhancement of mDia2 activity by Rho-kinase-dependent phosphorylation of the diaphanous autoregulatory domain. *Biochem. J.* **439,** 57-65 (2011). 10.1042/BJ20101700.
68. Guilluy C*, et al.*, The Rho GEFs LARG and GEF-H1 regulate the mechanical response to force on integrins. *Nat. Cell Biol.* **13,** 722-727 (2011). 10.1038/ncb2254.
69. Lawson CD & Burridge K, The on-off relationship of Rho and Rac during integrin-mediated adhesion and cell migration. *Small GTPases* **5,** e27958 (2014). 10.4161/sgtp.27958.
70. Saci A & Carpenter CL, RhoA GTPase regulates B cell receptor signaling. *Mol. Cell* **17,** 205-214 (2005). 10.1016/j.molcel.2004.12.012.
71. Saez de Guinoa J, Barrio L, Mellado M, & Carrasco YR, CXCL13/CXCR5 signaling enhances BCR-triggered B-cell activation by shaping cell dynamics. *Blood* **118,** 1560-1569 (2011). 10.1182/blood-2011-01-332106.
72. Merino-Cortes SV*, et al.*, Diacylglycerol kinase zeta promotes actin cytoskeleton remodeling and mechanical forces at the B cell immune synapse. *Sci. Signal.* **13,** (2020). 10.1126/scisignal.aaw8214.
73. Dustin ML, Chakraborty AK, & Shaw AS, Understanding the structure and function of the immunological synapse. *Cold Spring Harb. Perspect. Biol.* **2,** a002311 (2010). 10.1101/cshperspect.a002311.
74. Nordenfelt P, Elliott HL, & Springer TA, Coordinated integrin activation by actin-dependent force during T-cell migration. *Nat. Commun.* **7,** 13119 (2016). 10.1038/ncomms13119.
75. Parsons JT, Horwitz AR, & Schwartz MA, Cell adhesion: integrating cytoskeletal dynamics and cellular tension. *Nat. Rev. Mol. Cell Biol.* **11,** 633-643 (2010). 10.1038/nrm2957.
76. Comrie WA, Li S, Boyle S, & Burkhardt JK, The dendritic cell cytoskeleton promotes T cell adhesion and activation by constraining ICAM-1 mobility. *J. Cell Biol.* **208,** 457-473 (2015). 10.1083/jcb.201406120.
77. Natkanski E*, et al.*, B cells use mechanical energy to discriminate antigen affinities. *Science* **340,** 1587-1590 (2013). 10.1126/science.1237572.
78. Spillane KM & Tolar P, Mechanics of antigen extraction in the B cell synapse. *Mol. Immunol.* **101,** 319-328 (2018). 10.1016/j.molimm.2018.07.018.
79. Hoogeboom R*, et al.*, Myosin IIa Promotes Antibody Responses by Regulating B Cell Activation, Acquisition of Antigen, and Proliferation. *Cell Rep.* **23,** 2342-2353 (2018). 10.1016/j.celrep.2018.04.087.

80. Roper SI*, et al.*, B cells extract antigens at Arp2/3-generated actin foci interspersed with linear filaments. *Elife* **8,** (2019). 10.7554/eLife.48093.
81. Spillane KM & Tolar P, B cell antigen extraction is regulated by physical properties of antigen-presenting cells. *J. Cell Biol.* **216,** 217-230 (2017). 10.1083/jcb.201607064.
82. Huang WYC*, et al.*, A molecular assembly phase transition and kinetic proofreading modulate Ras activation by SOS. *Science* **363,** 1098-1103 (2019). 10.1126/science.aau5721.
83. Hwang IY*, et al.*, An essential role for RGS protein/Galphai2 interactions in B lymphocyte-directed cell migration and trafficking. *J. Immunol.* **194,** 2128-2139 (2015). 10.4049/jimmunol.1401952.
84. Alexander CJ & Hammer JA, 3rd, Optimization of cerebellar purkinje neuron cultures and development of a plasmid-based method for purkinje neuron-specific, miRNA-mediated protein knockdown. *Methods Cell Biol.* **131,** 177-197 (2016). 10.1016/bs.mcb.2015.06.004.
85. Hong J, Murugesan S, Betzig E, & Hammer JA, Contractile actomyosin arcs promote the activation of primary mouse T cells in a ligand-dependent manner. *PLoS One* **12,** e0183174 (2017). 10.1371/journal.pone.0183174.
86. Comrie WA, Babich A, & Burkhardt JK, F-actin flow drives affinity maturation and spatial organization of LFA-1 at the immunological synapse. *J. Cell Biol.* **208,** 475-491 (2015). 10.1083/jcb.201406121.
87. Jaumouille V, Cartagena-Rivera AX, & Waterman CM, Coupling of beta2 integrins to actin by a mechanosensitive molecular clutch drives complement receptor-mediated phagocytosis. *Nat. Cell Biol.* **21,** 1357-1369 (2019). 10.1038/s41556-019-0414-2.
88. Martiel JL*, et al.*, Measurement of cell traction forces with ImageJ. *Methods Cell Biol.* **125,** 269-287 (2015). 10.1016/bs.mcb.2014.10.008.
89. Burgess A*, et al.*, Loss of human Greatwall results in G2 arrest and multiple mitotic defects due to deregulation of the cyclin B-Cdc2/PP2A balance. *Proc. Natl. Acad. Sci.* **107,** 12564-12569 (2010). 10.1073/pnas.0914191107.
90. Tinevez JY*, et al.*, TrackMate: An open and extensible platform for single-particle tracking. *Methods* **115,** 80-90 (2017). 10.1016/j.ymeth.2016.09.016.

Figure 1

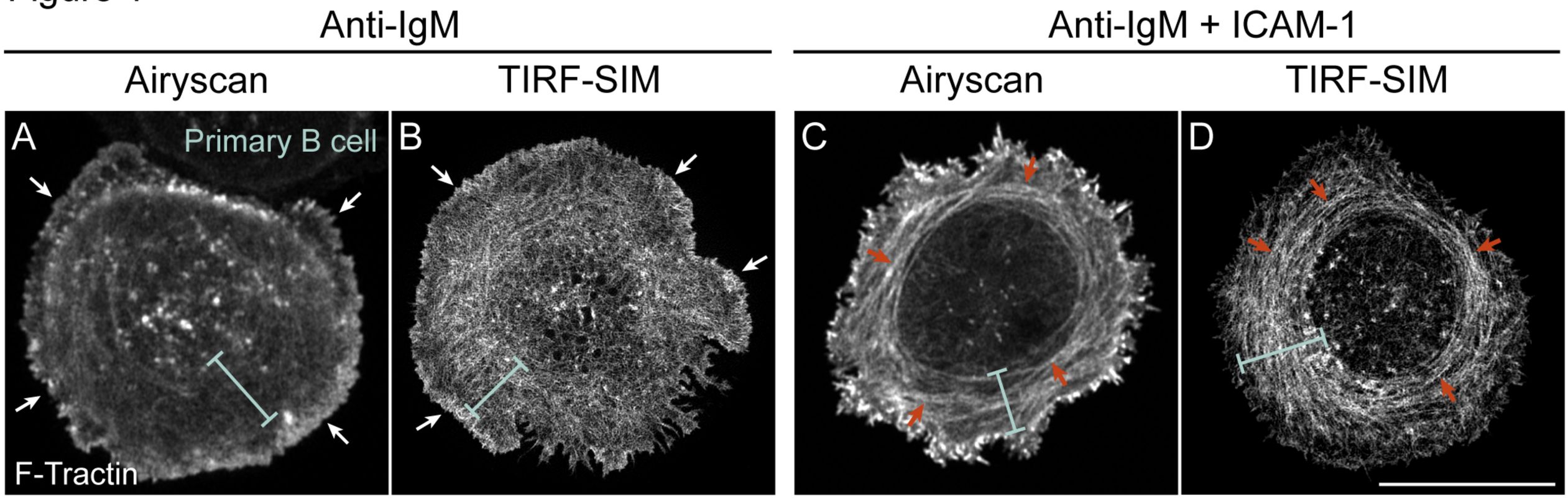

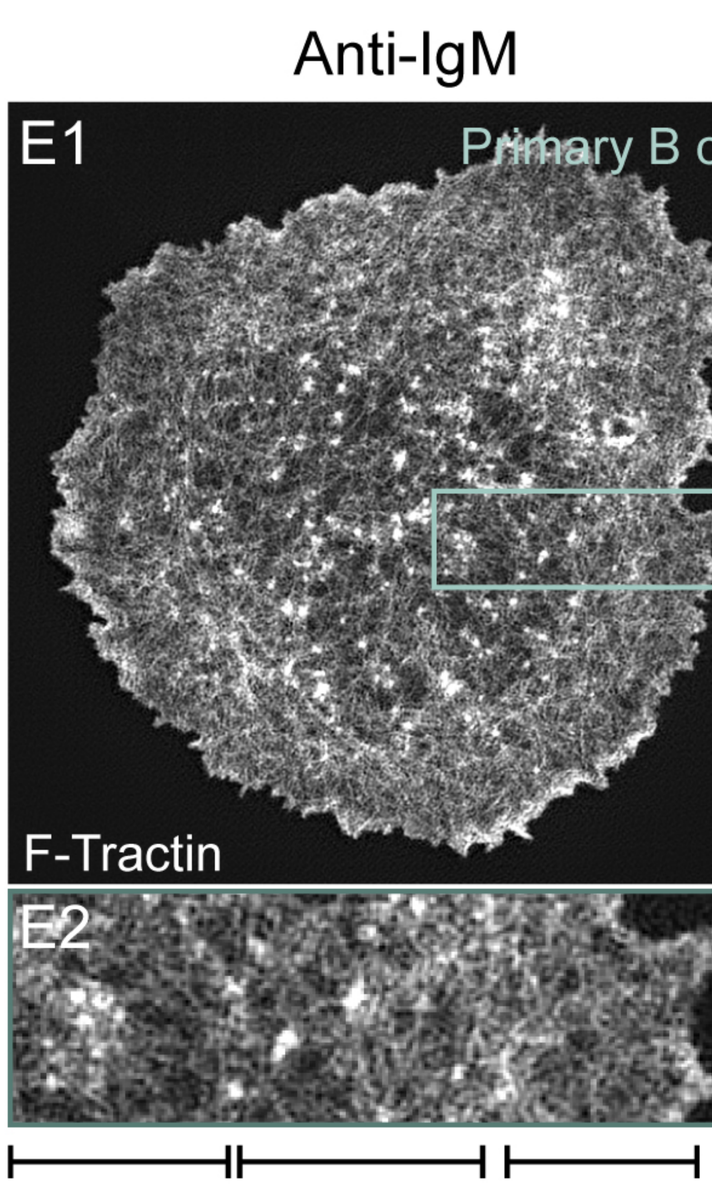

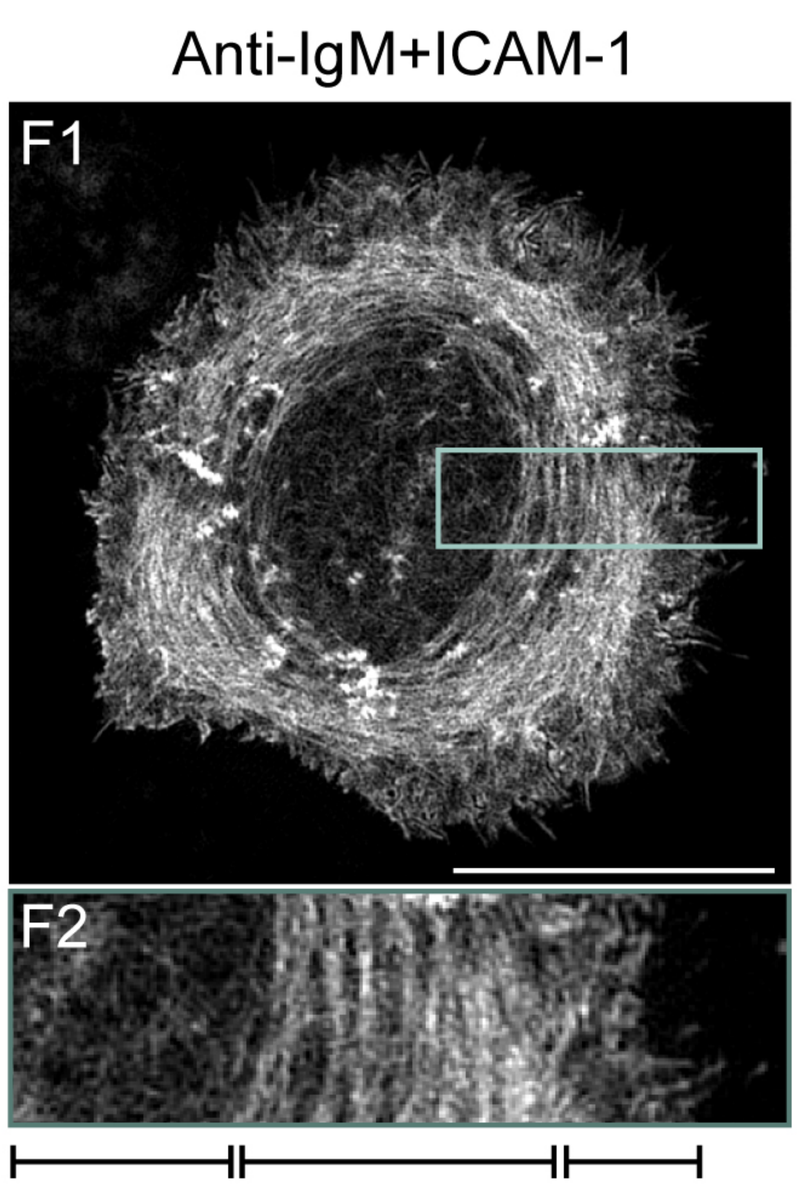

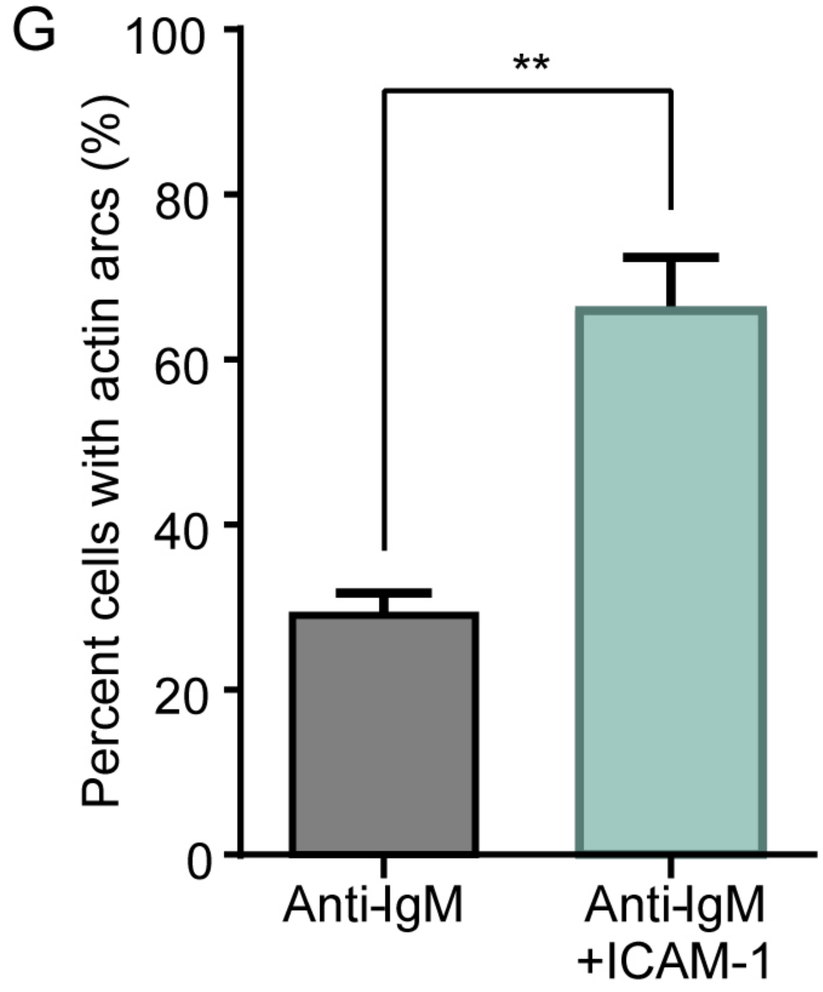

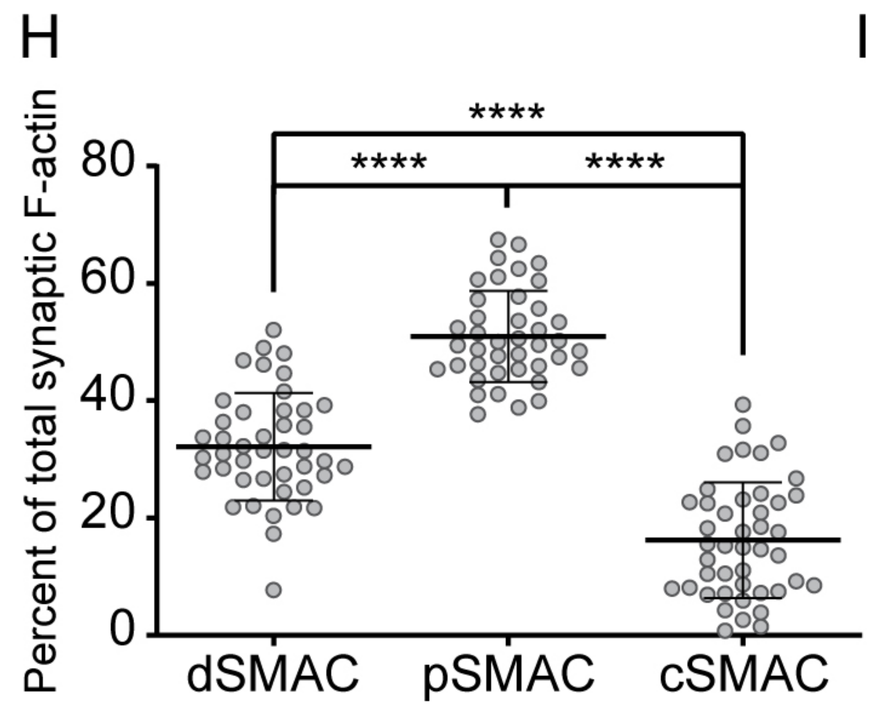

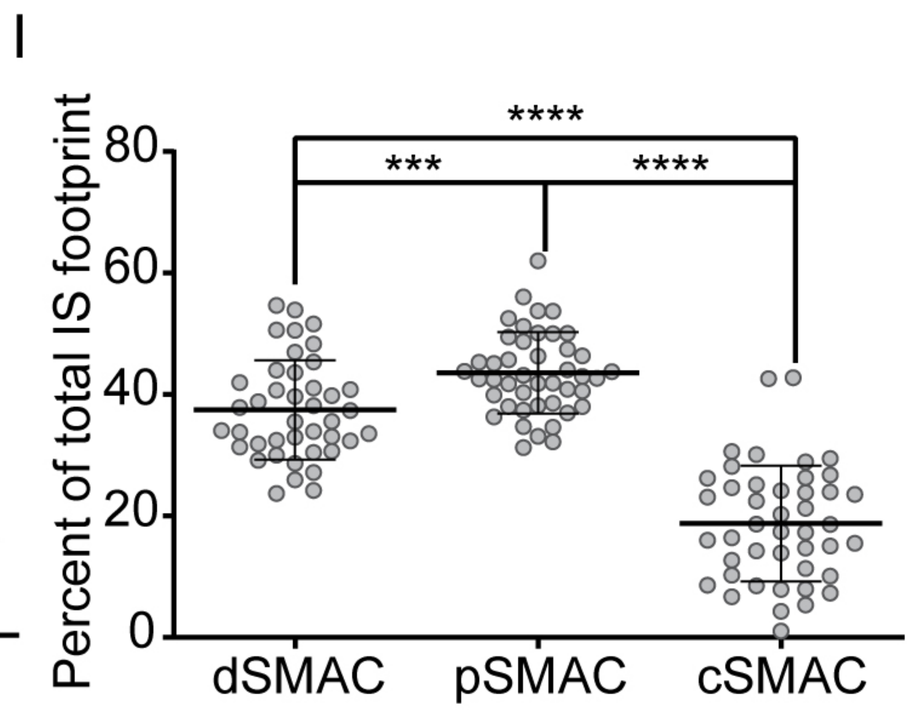

Figure 2

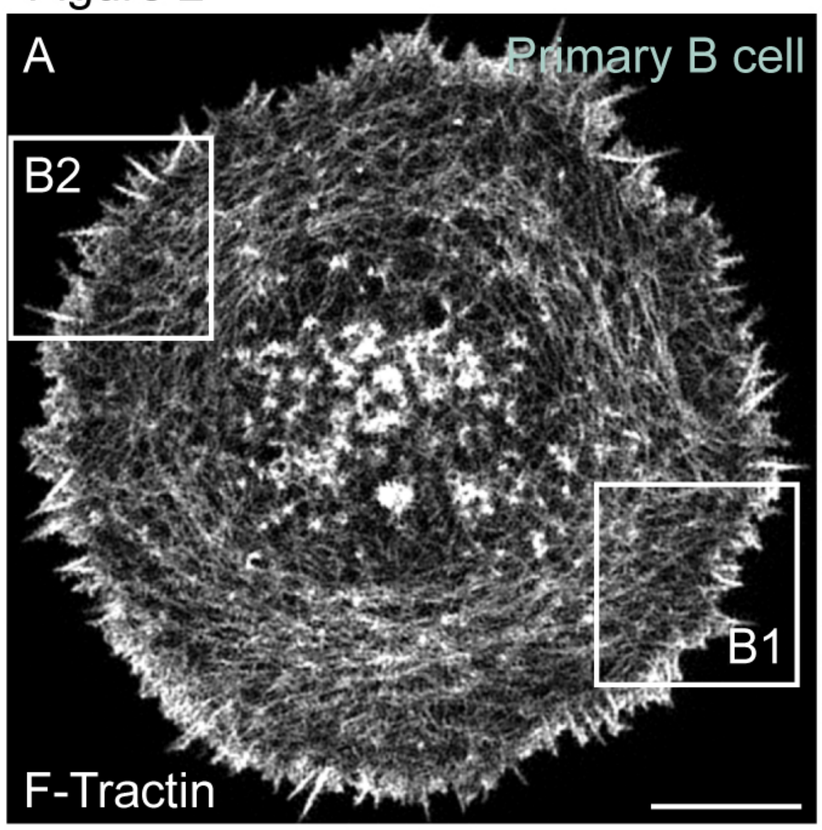

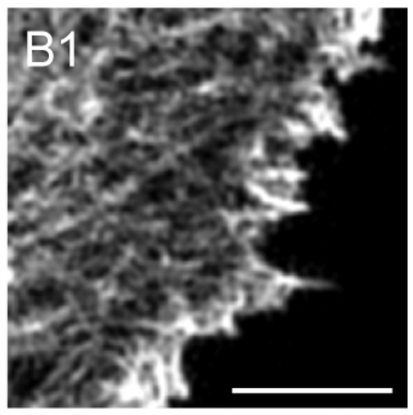

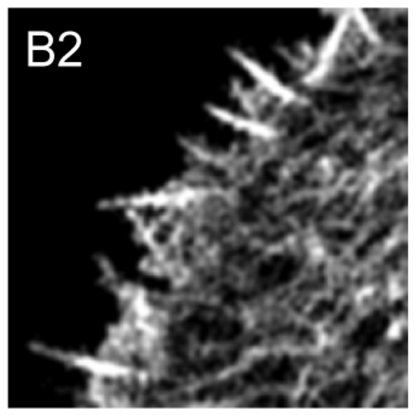

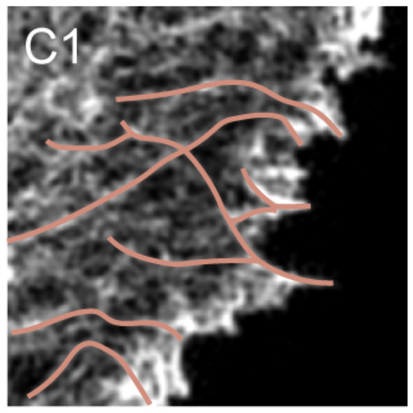

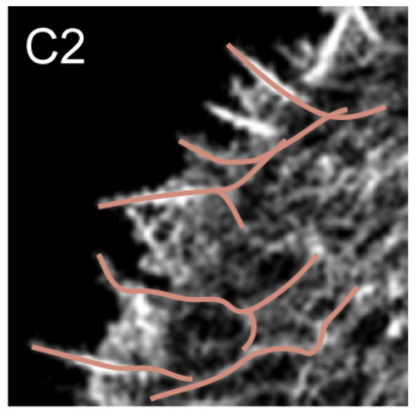

Before SMIFH2 +SMIFH2 6'

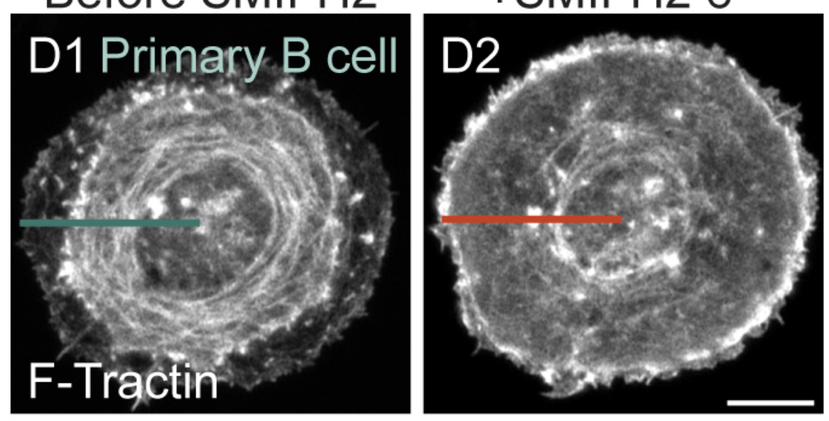

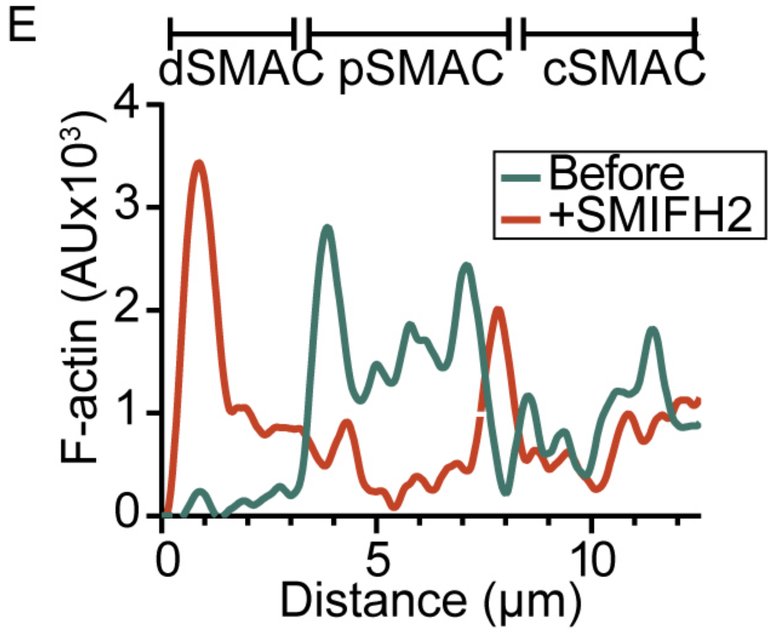

Vector miRNA#1 miRNA#2 miRNA#3

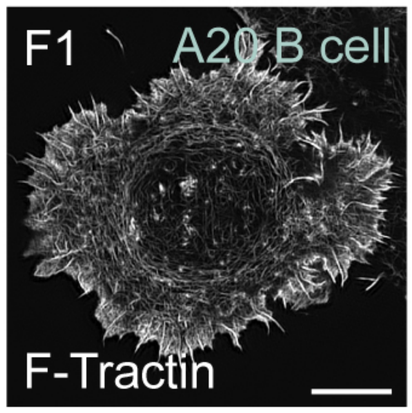

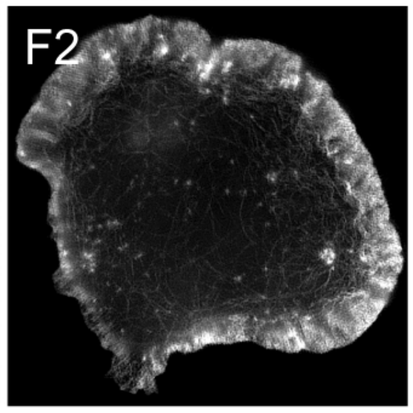

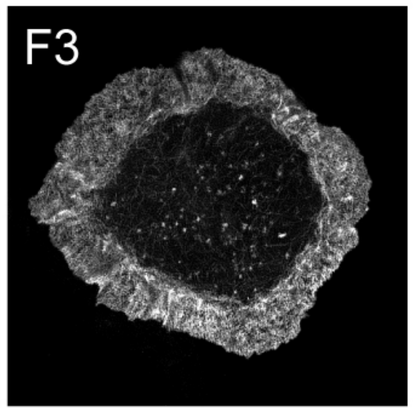

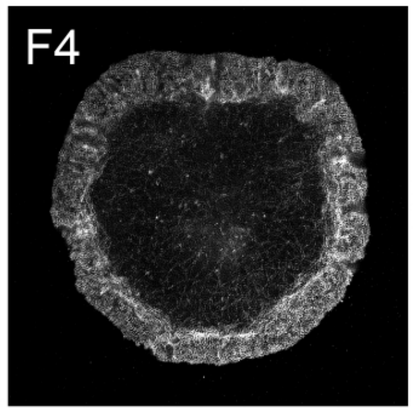

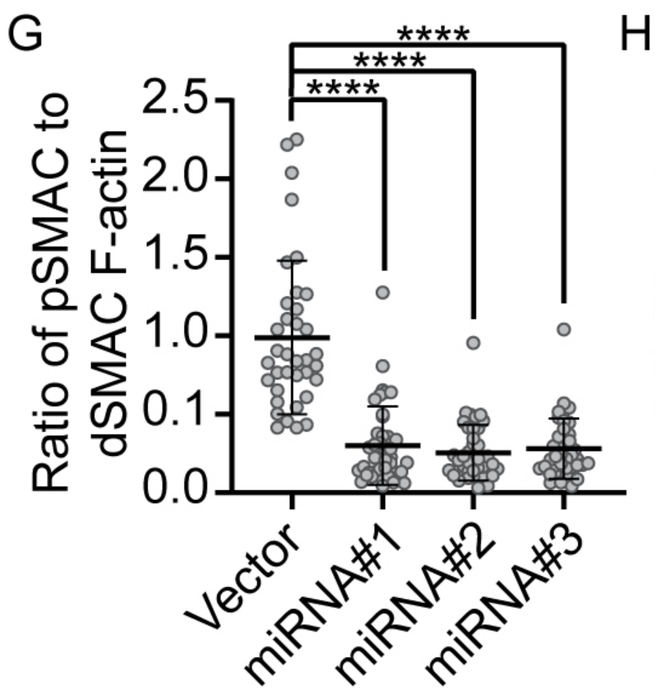

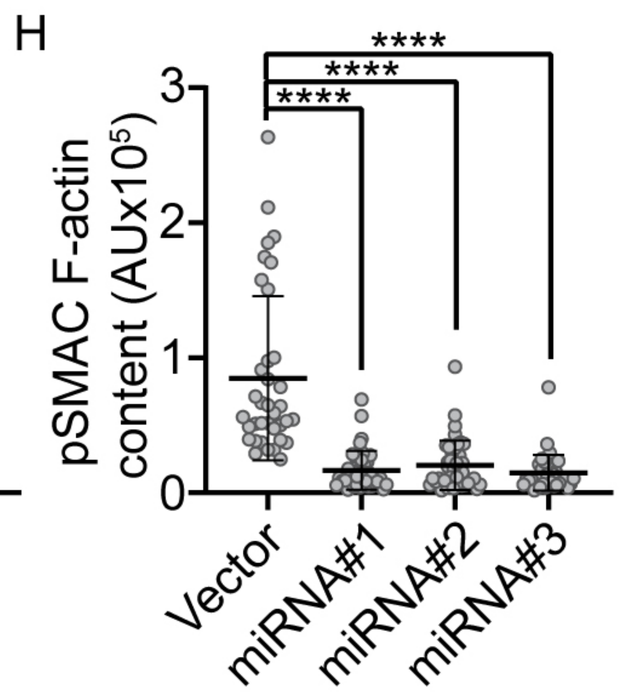

Figure 3

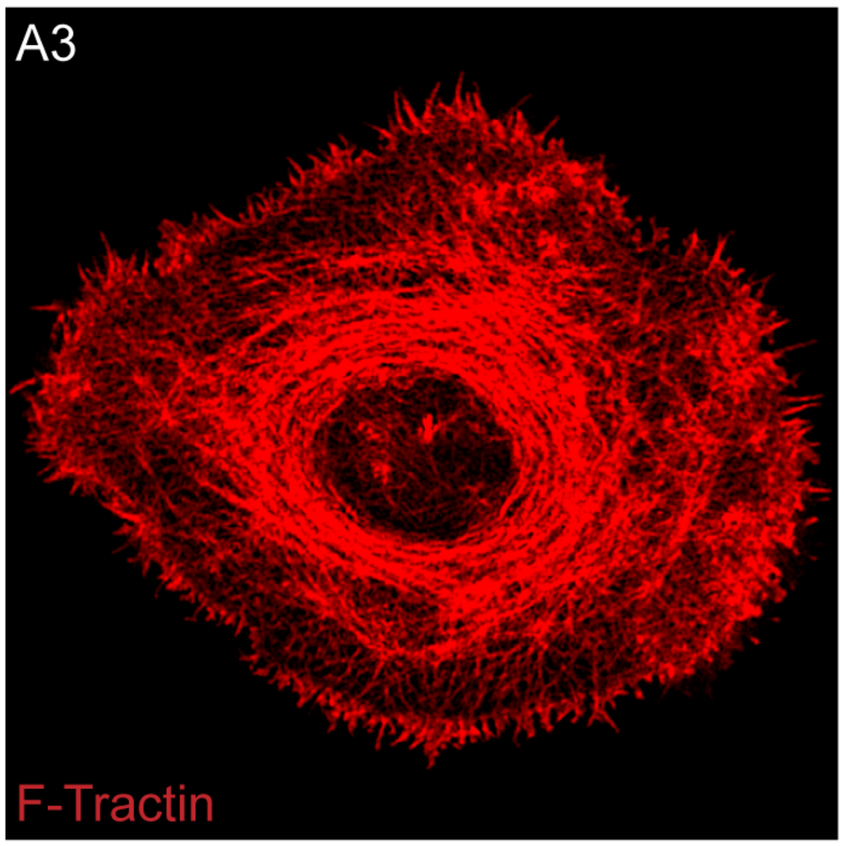
A3
F-Tractin

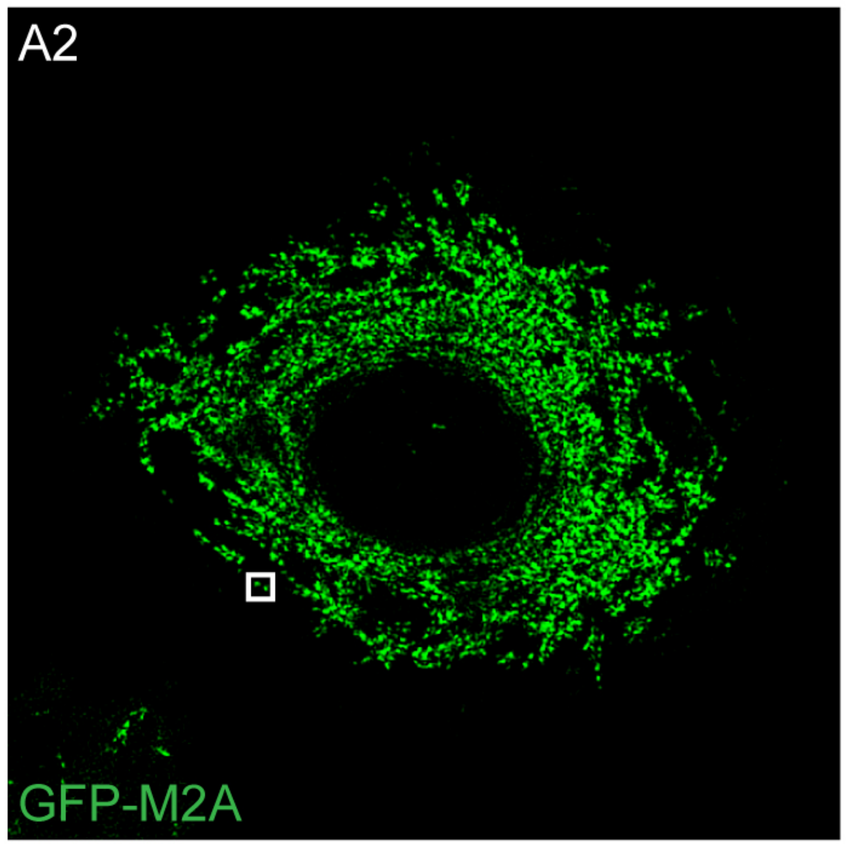
A2
GFP-M2A

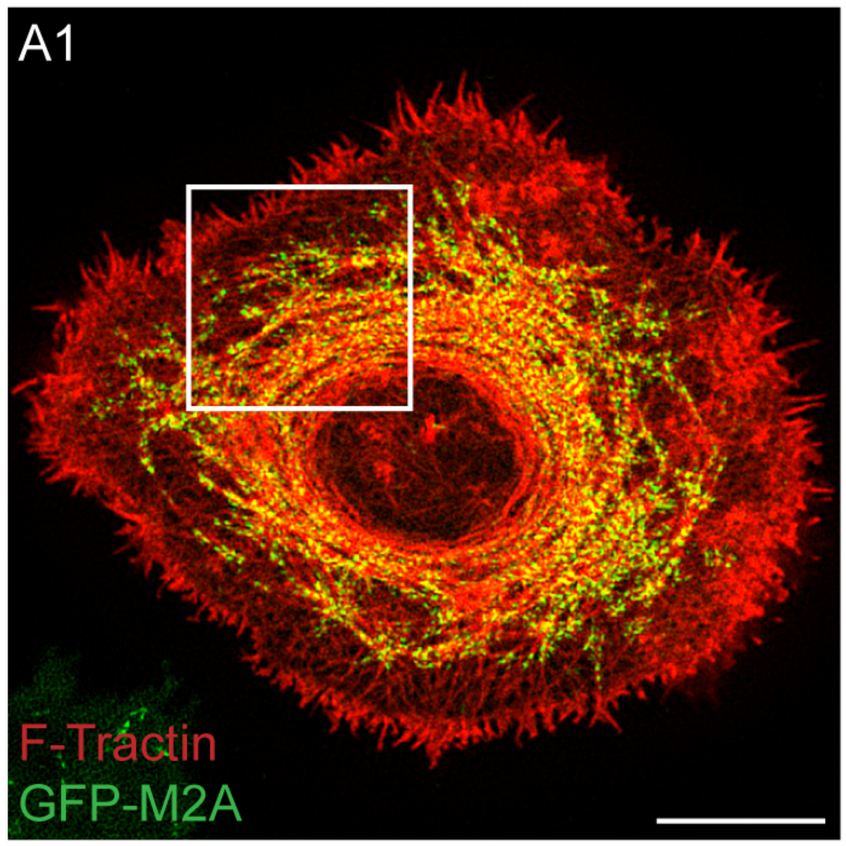
A1
F-Tractin
GFP-M2A

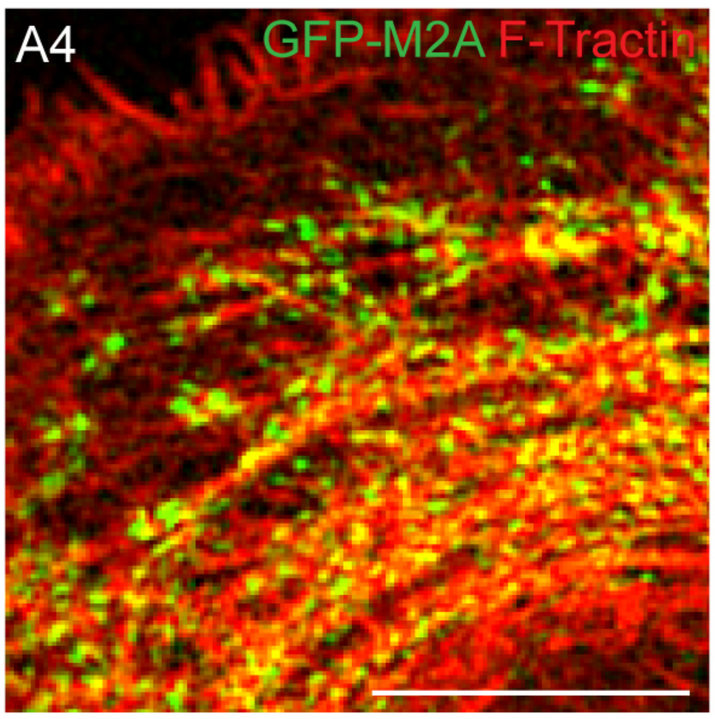
A4
GFP-M2A F-Tractin

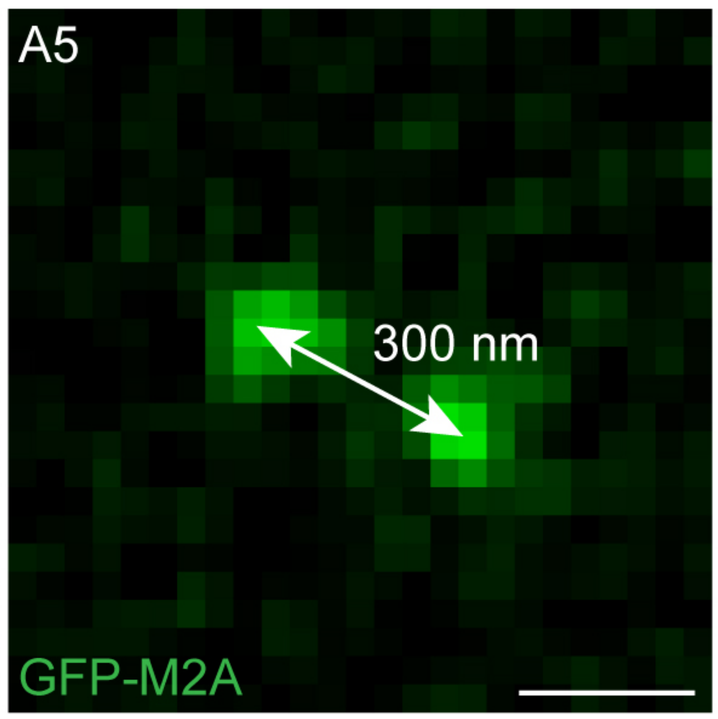
A5
300 nm
GFP-M2A

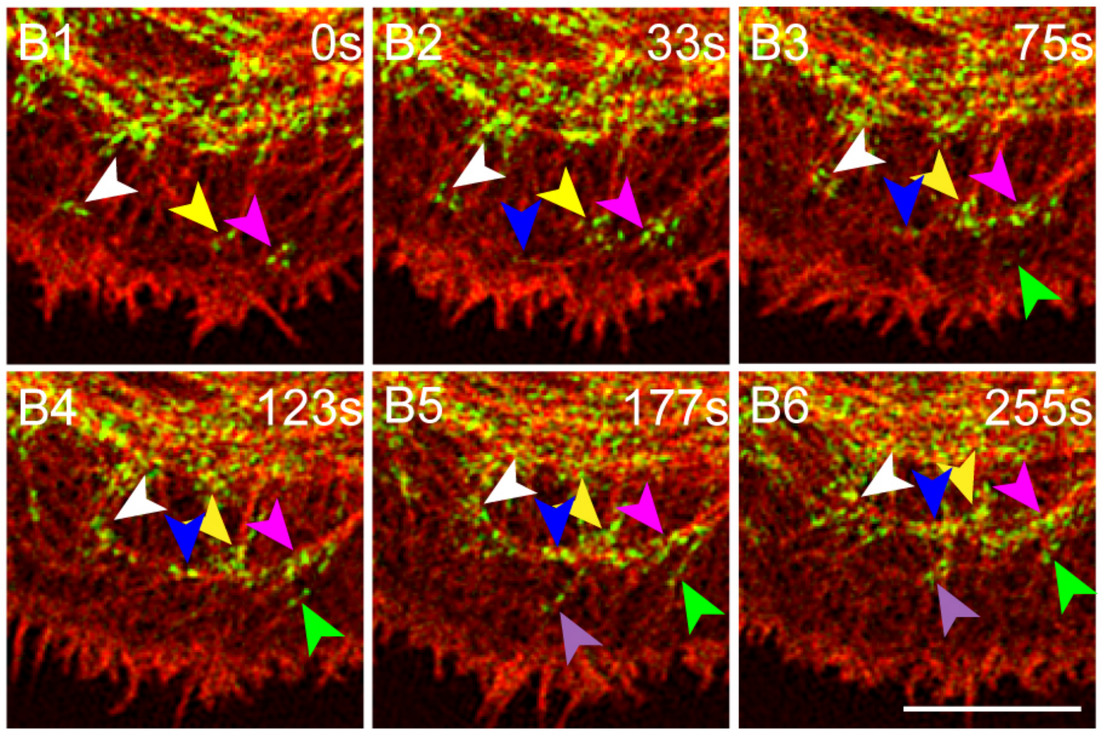
B1
0s
B2
33s
B3
75s
B4
123s
B5
177s
B6
255s

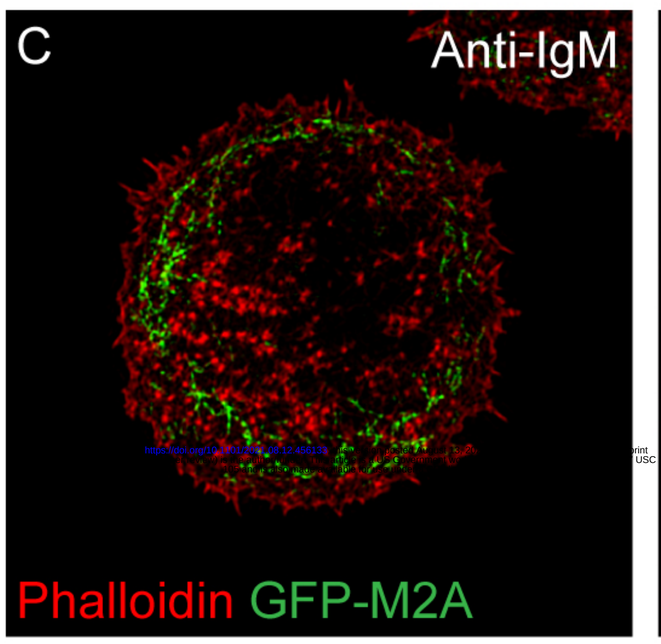
C
Anti-IgM
Phalloidin GFP-M2A

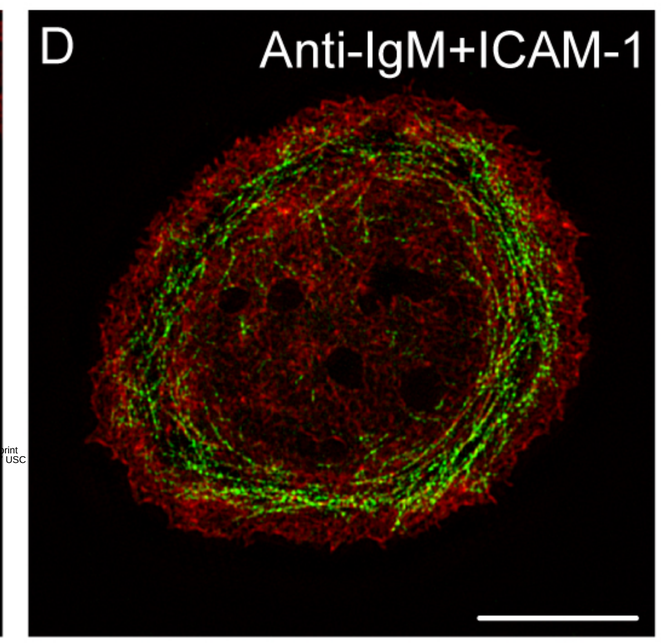
D
Anti-IgM+ICAM-1

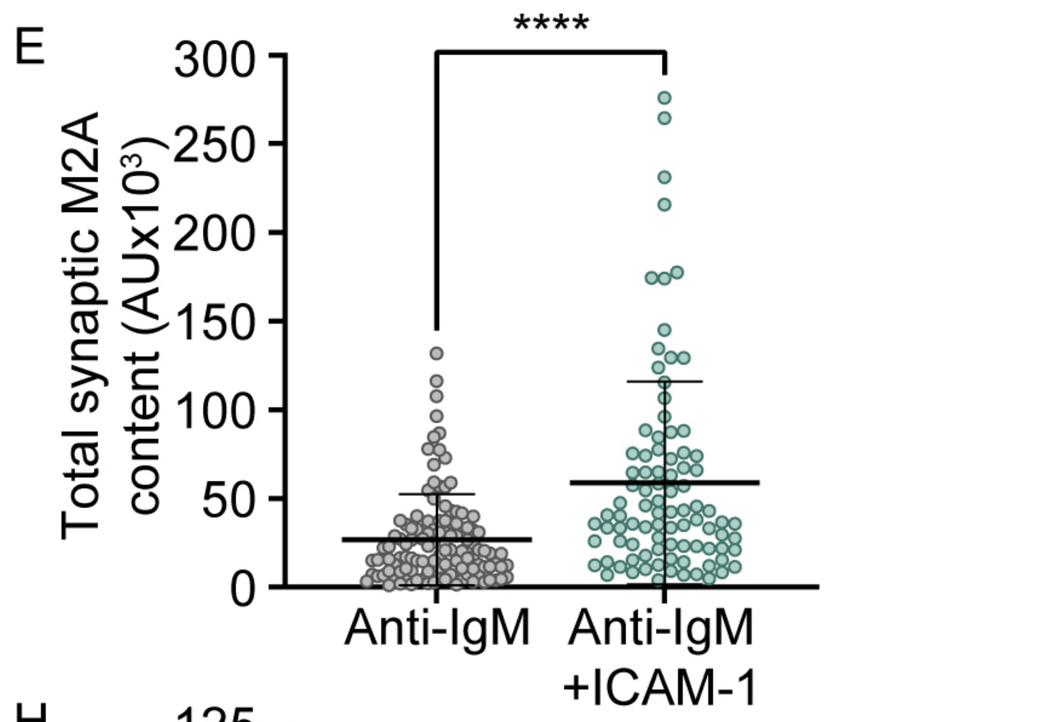
E
****
Total synaptic M2A content (AUx10³)
300
250
200
150
100
50
0
Anti-IgM
Anti-IgM +ICAM-1

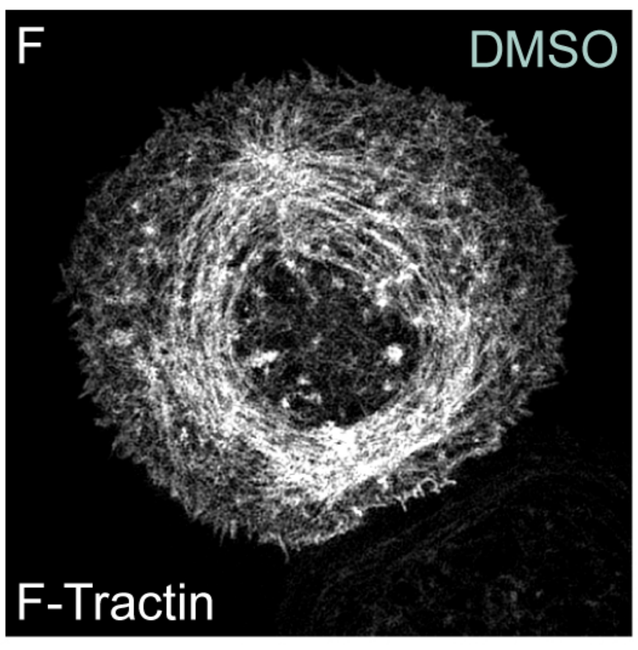
F
DMSO
F-Tractin

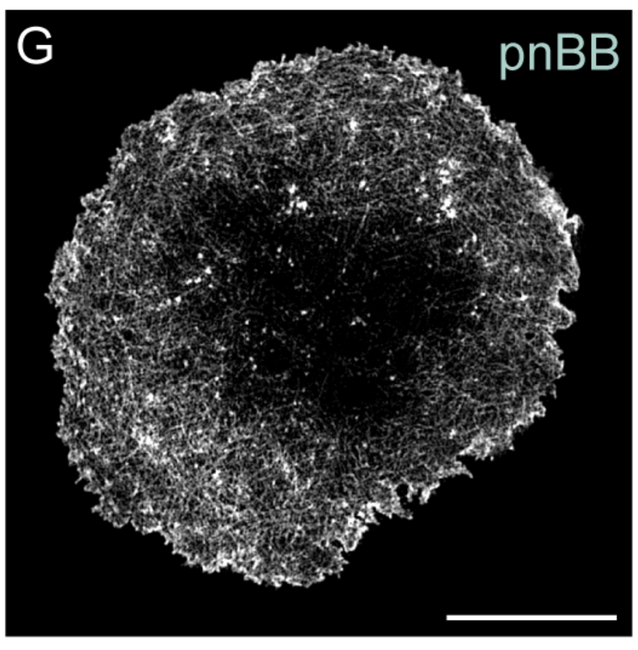
G
pnBB

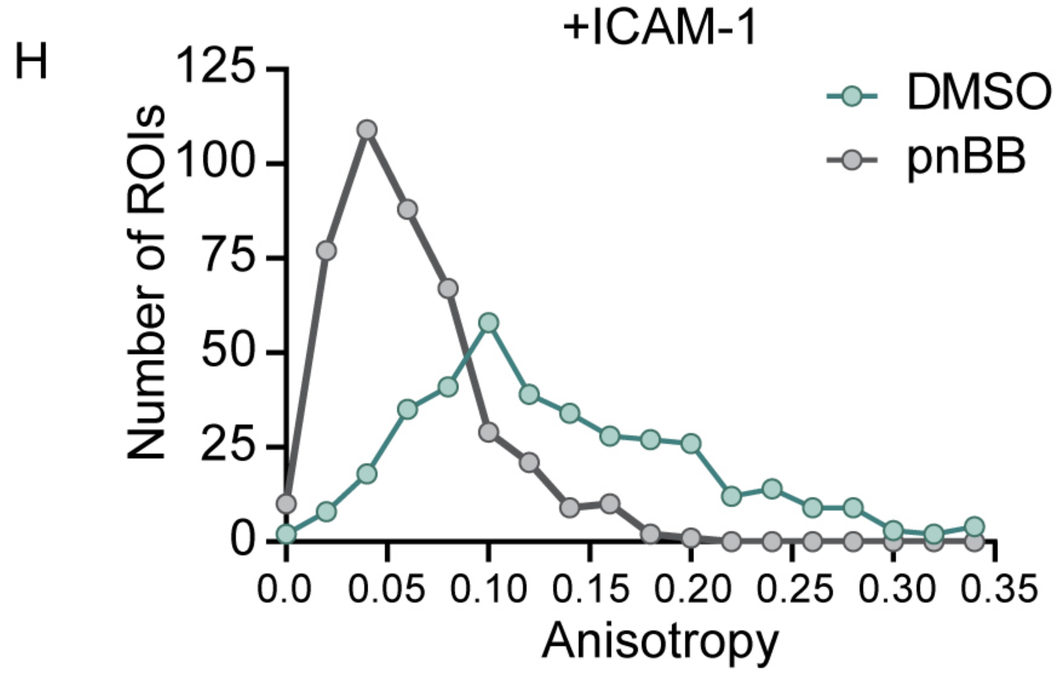
H
DMSO
pnBB
Number of ROIs
125
100
75
50
25
0
0.0
0.05
0.10
0.15
0.20
0.25
0.30
0.35
Anisotropy

Figure 4

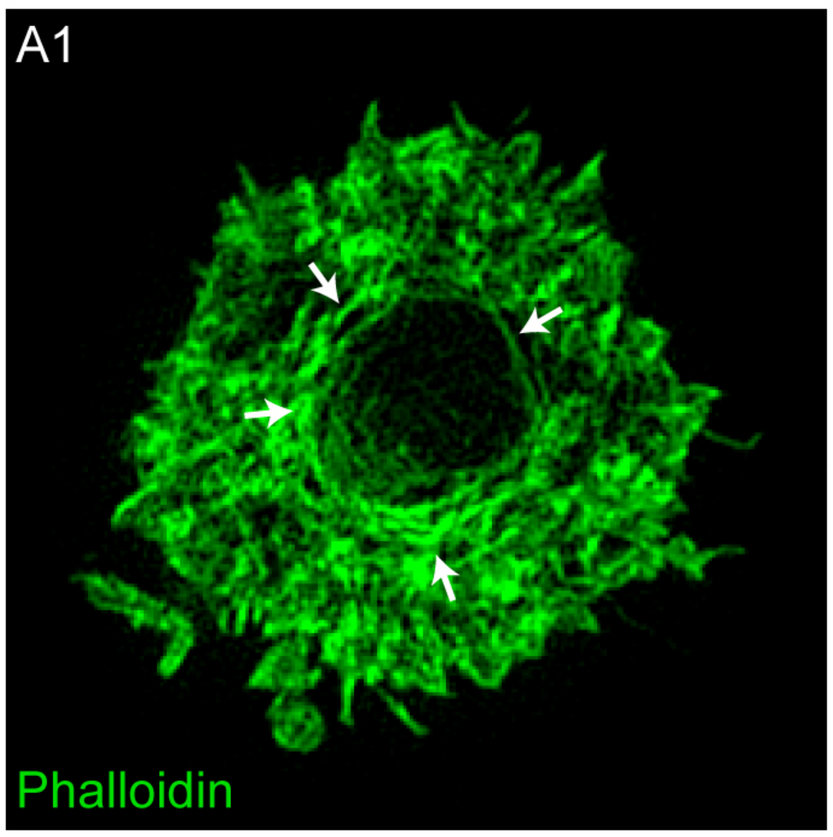

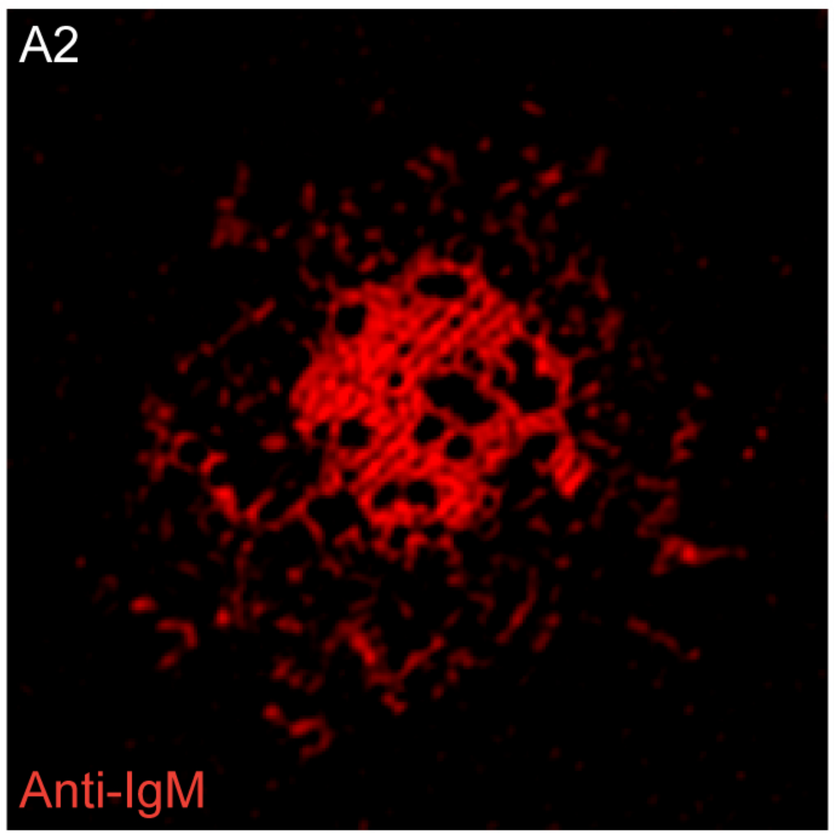

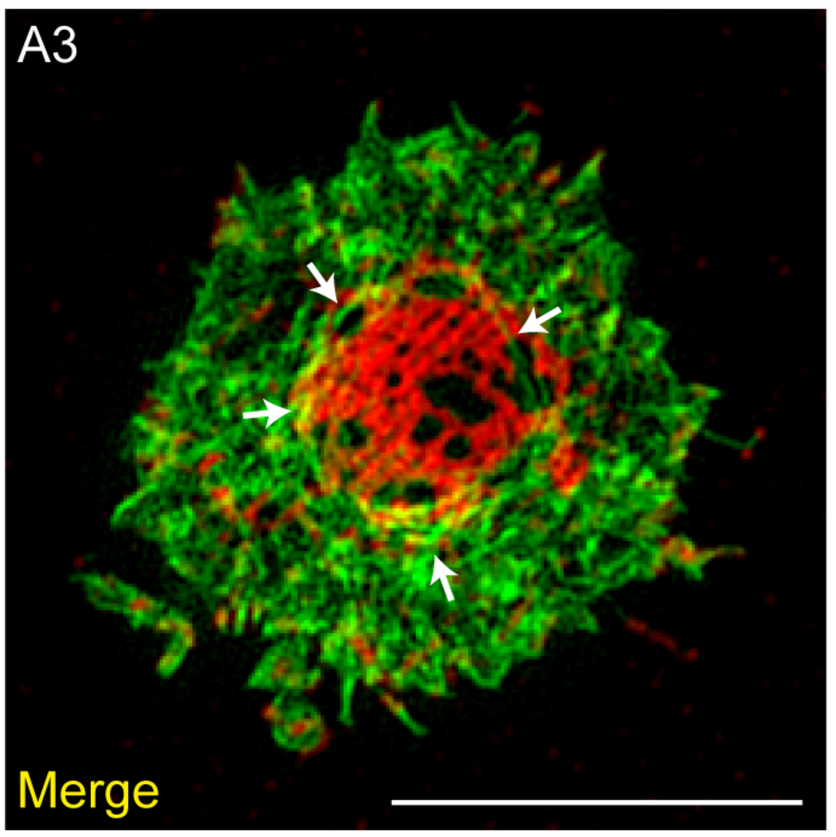

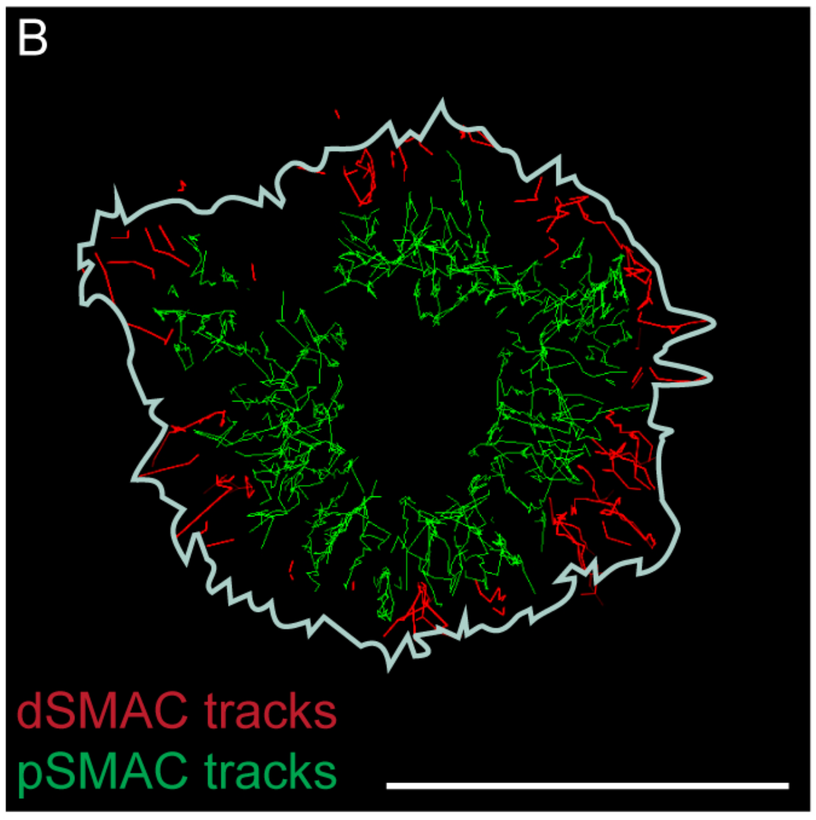

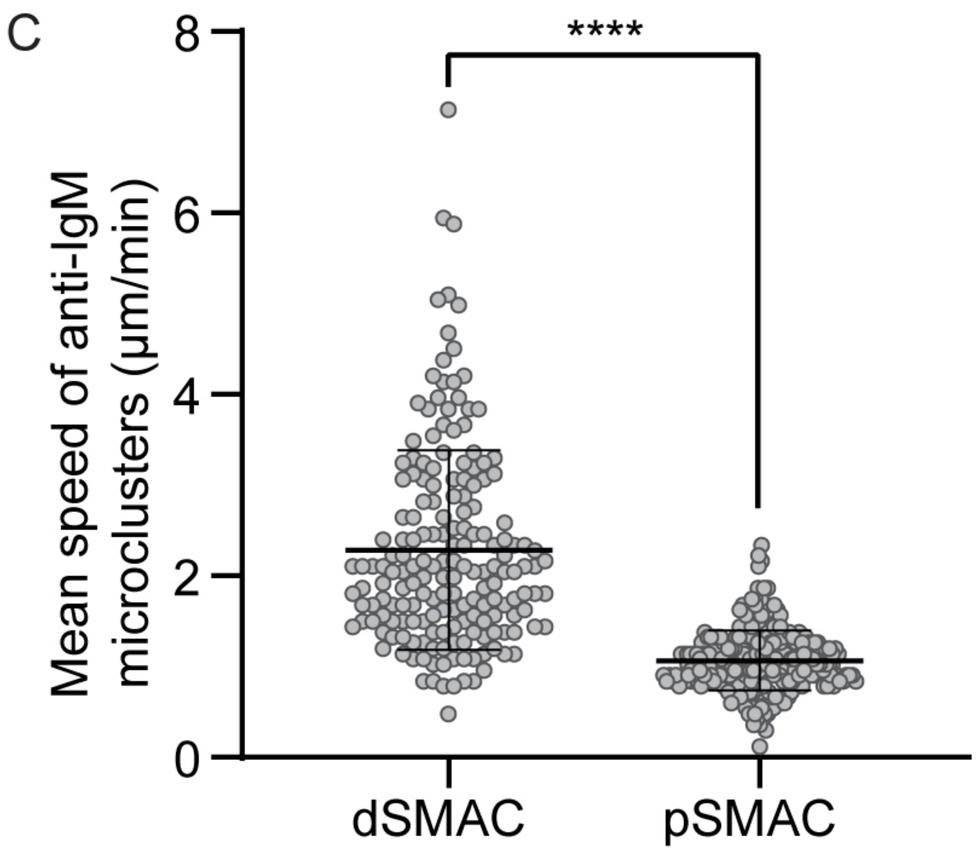

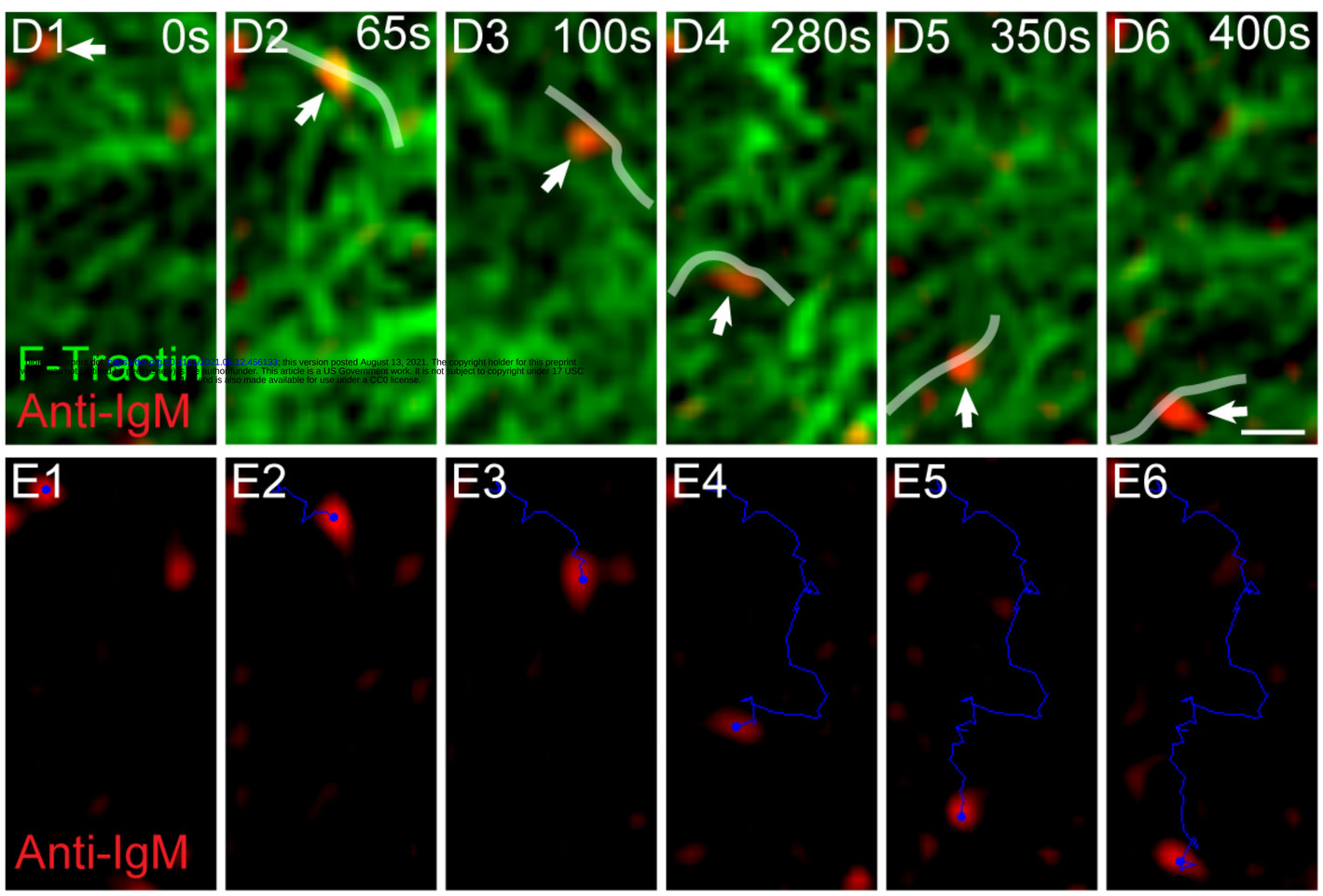

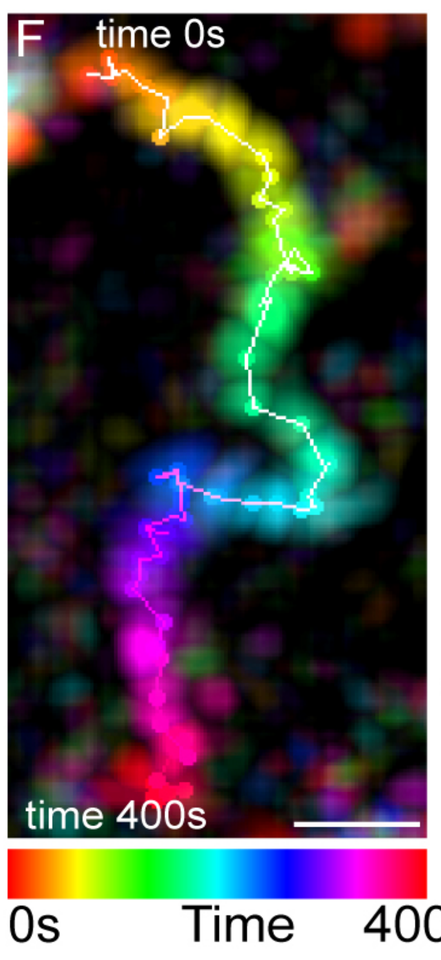

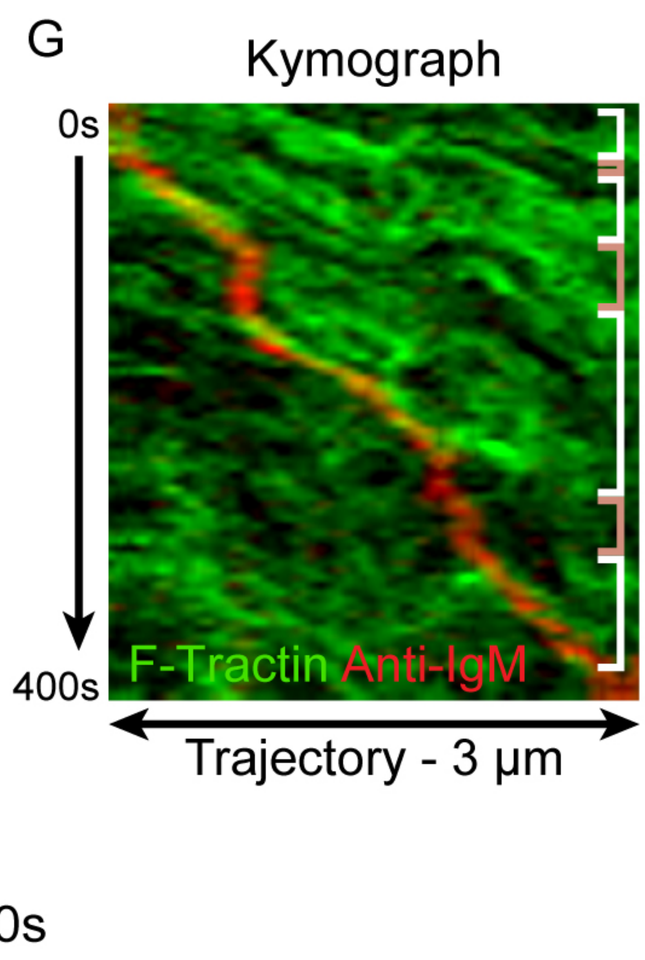

Figure 5

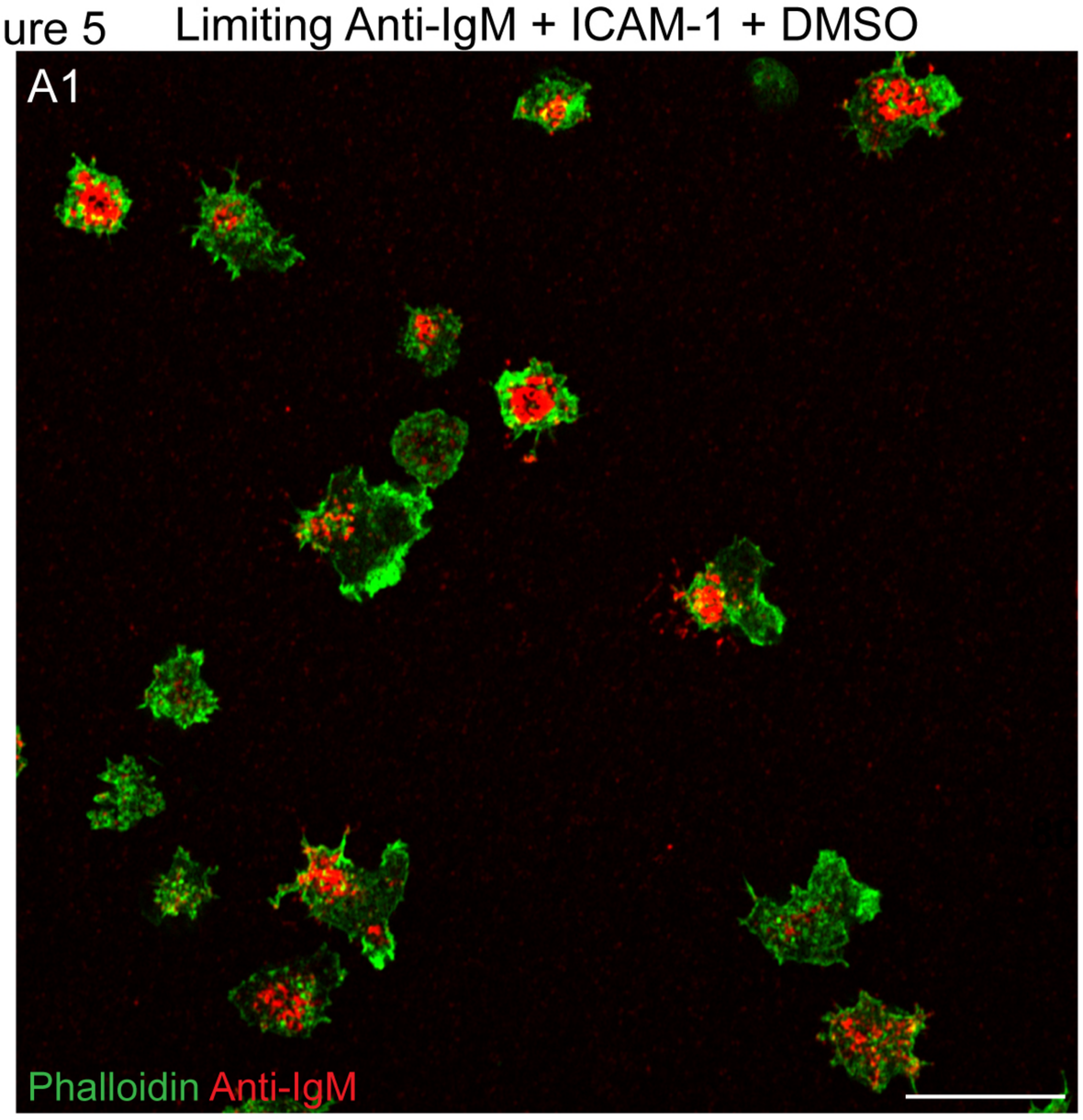
Limiting Anti-IgM + ICAM-1 + DMSO
A1
Phalloidin Anti-IgM
A2
Phalloidin
A3
Anti-IgM
Phalloidin
Anti-IgM
Merge
C1
C2
C3
DMSO
D1
D2
D3
pnBB

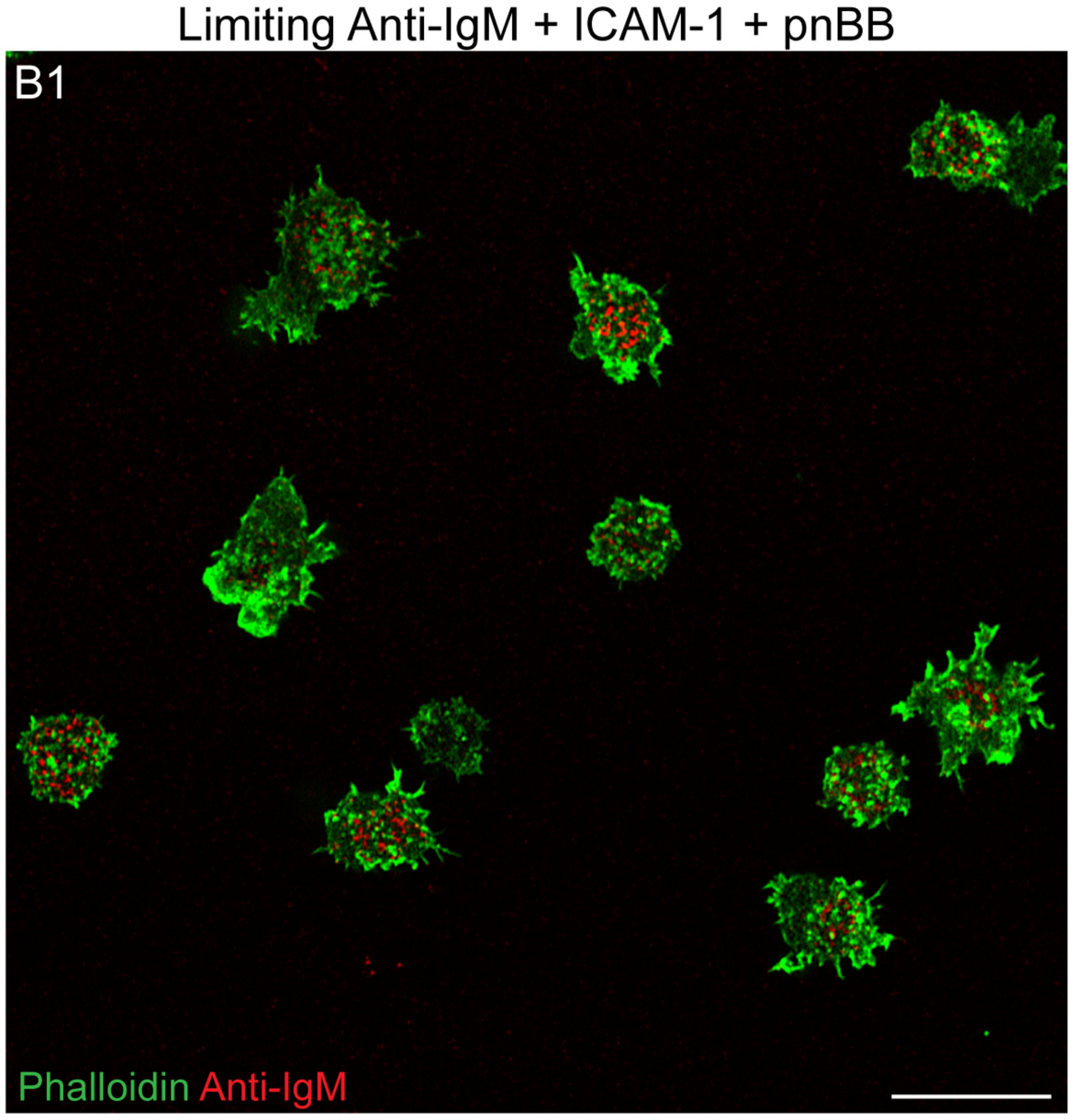
Limiting Anti-IgM + ICAM-1 + pnBB
B1
Phalloidin Anti-IgM
B2
Phalloidin
B3
Anti-IgM

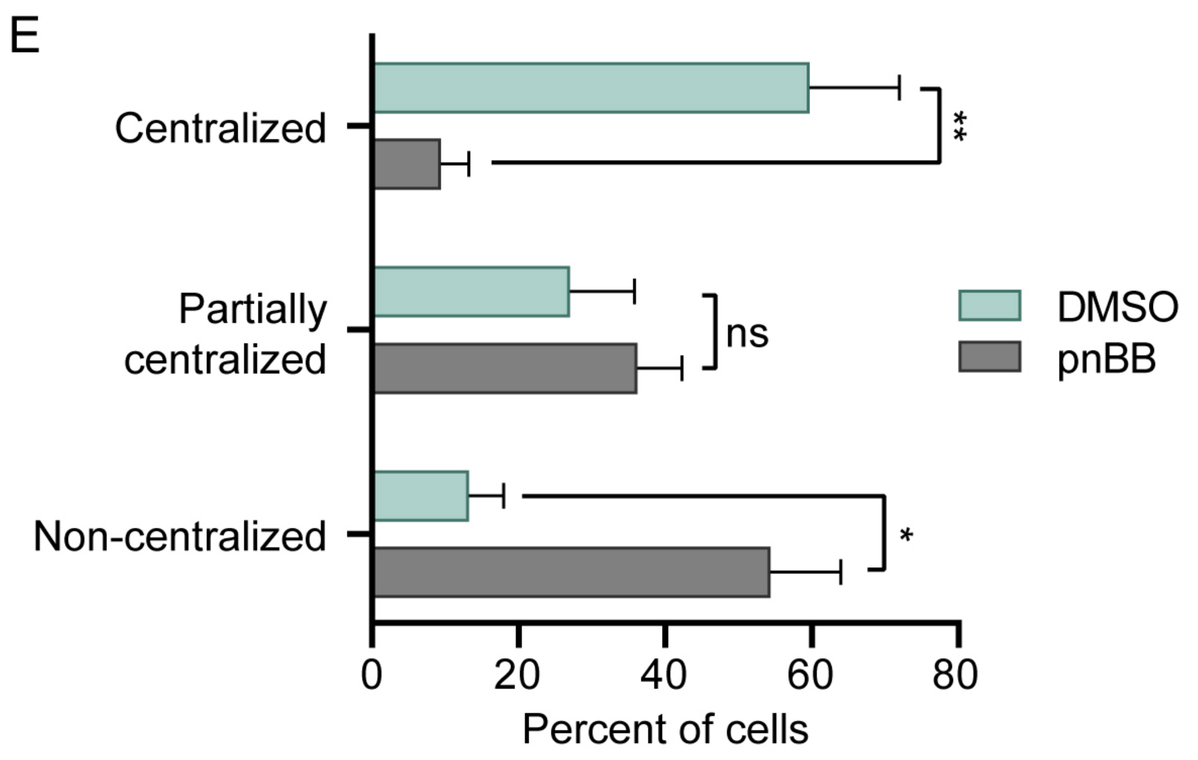
E
Centralized
Partially centralized
Non-centralized
**
ns
*
DMSO
pnBB
0
20
40
60
80
Percent of cells

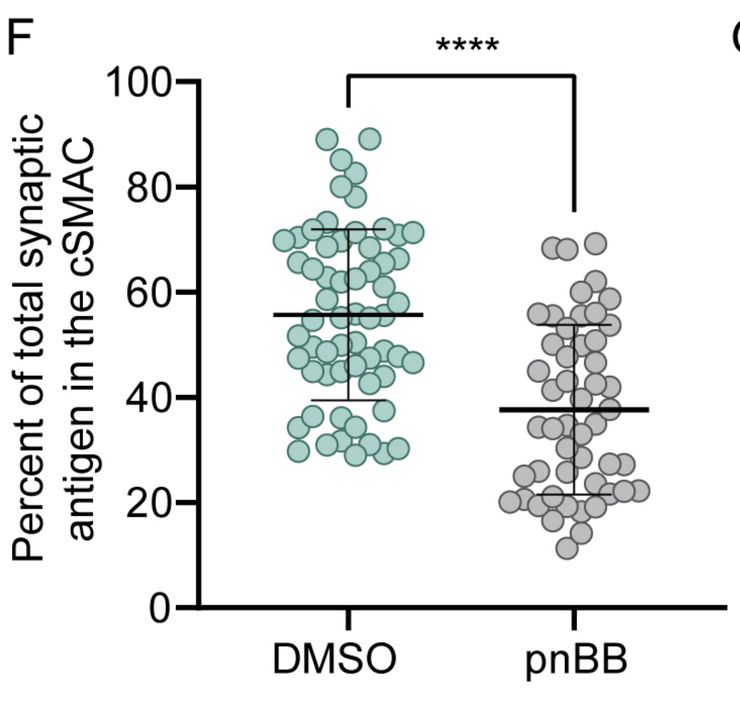
F
****
Percent of total synaptic antigen in the cSMAC
100
80
60
40
20
0
DMSO
pnBB

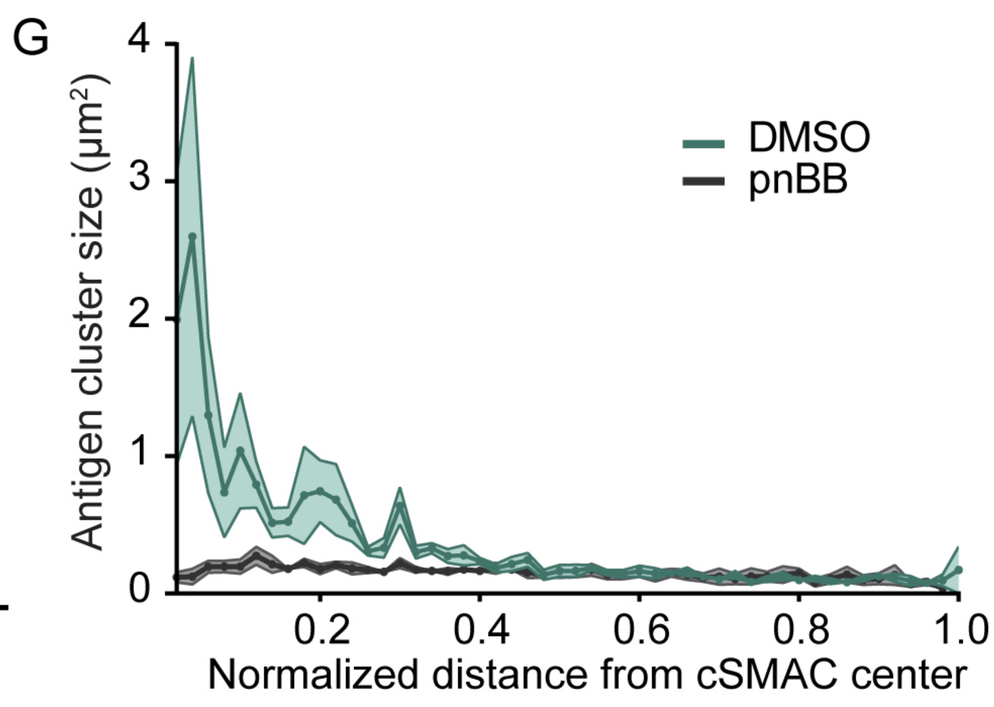
G
Antigen cluster size (μm²)
4
3
2
1
0
DMSO
pnBB
0.2
0.4
0.6
0.8
1.0
Normalized distance from cSMAC center

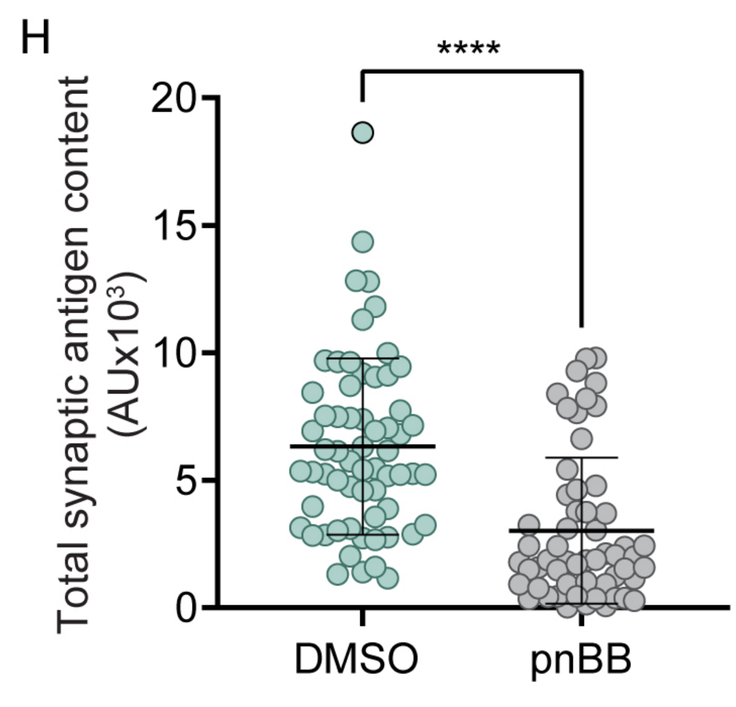
H
****
Total synaptic antigen content (AUx10³)
20
15
10
5
0
DMSO
pnBB

Figure 6

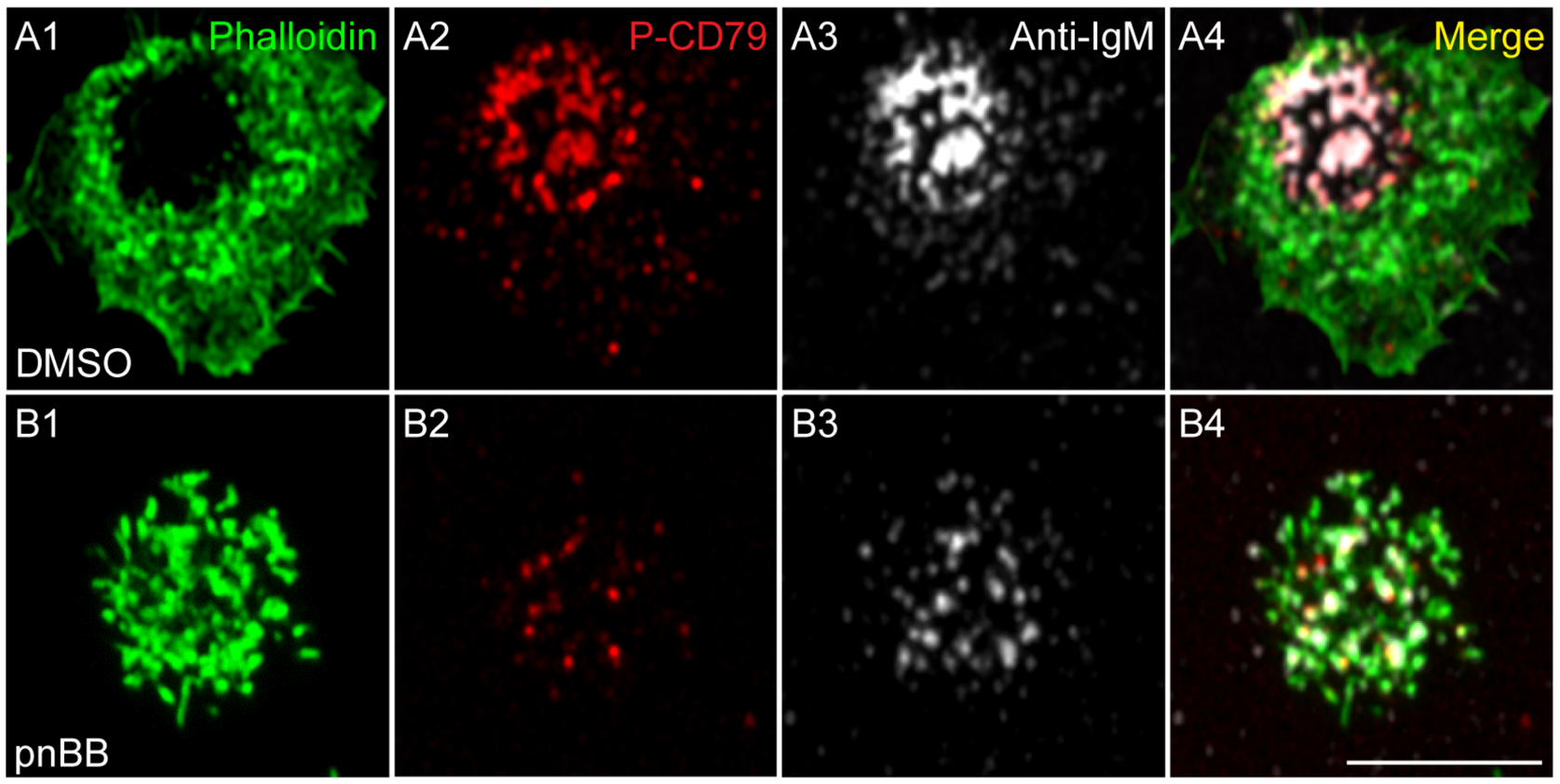

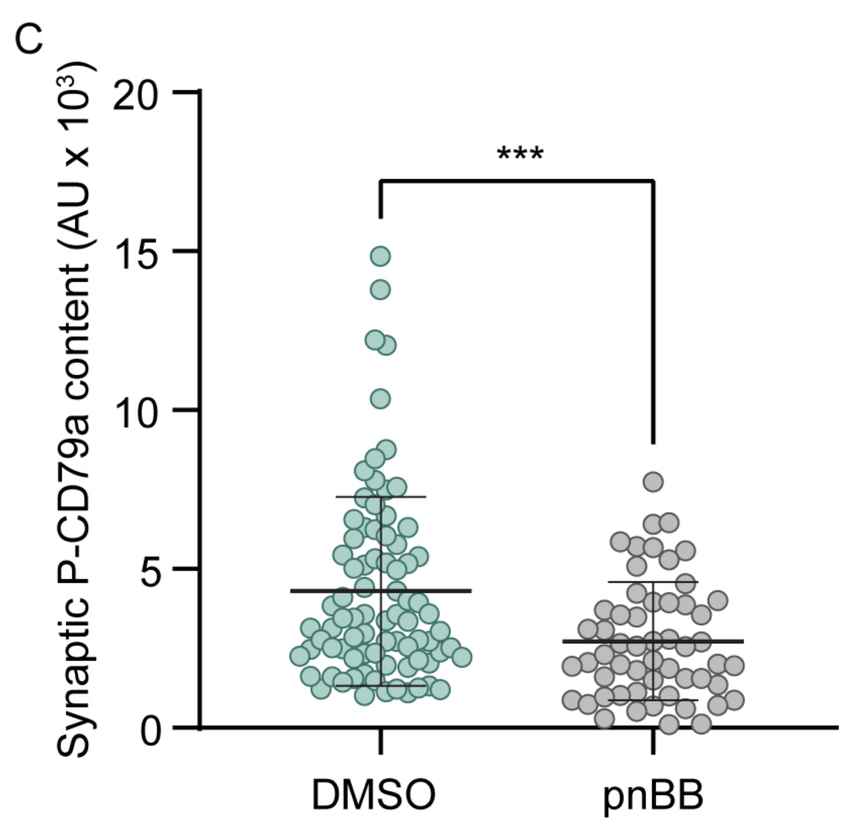

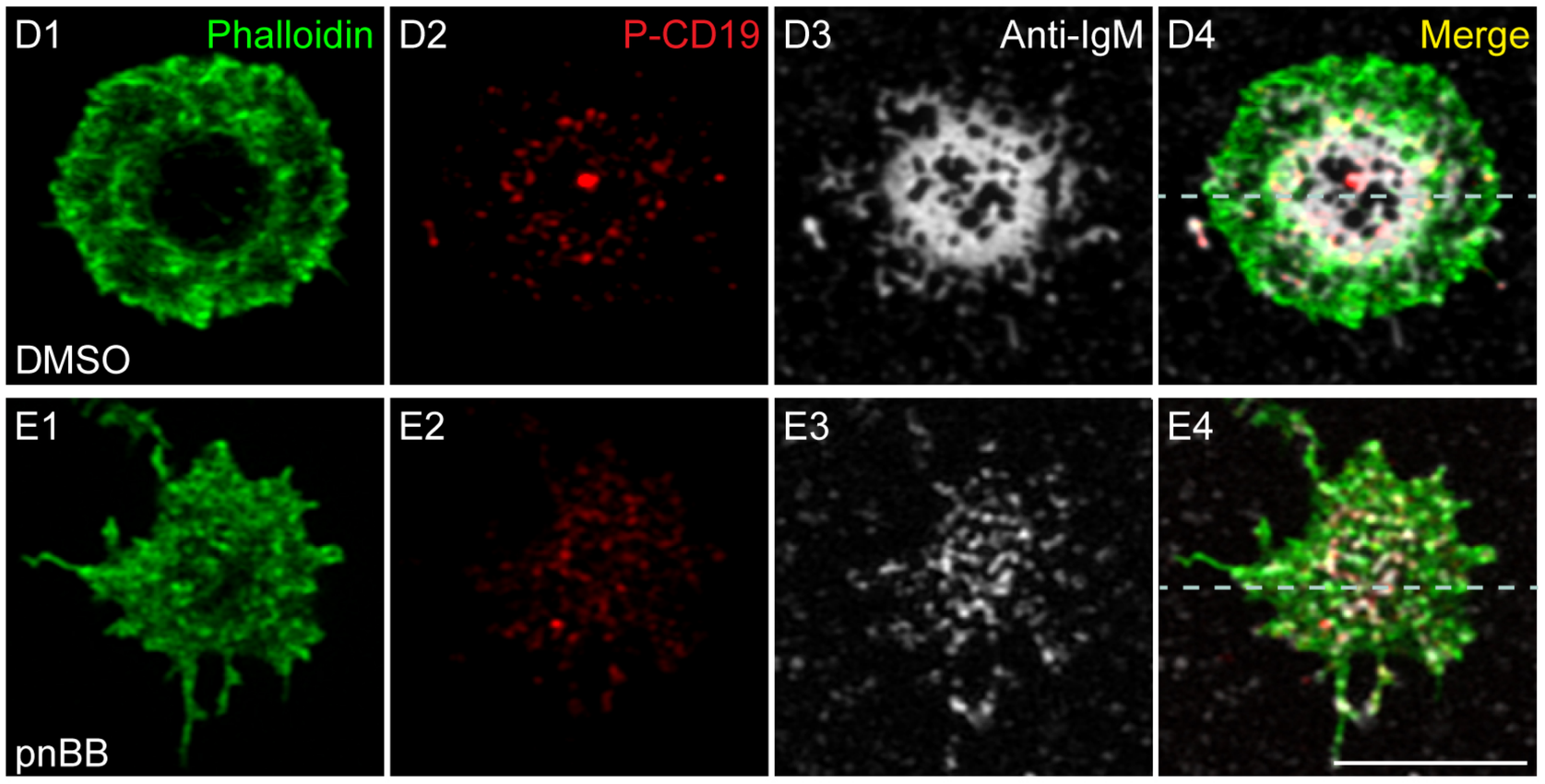

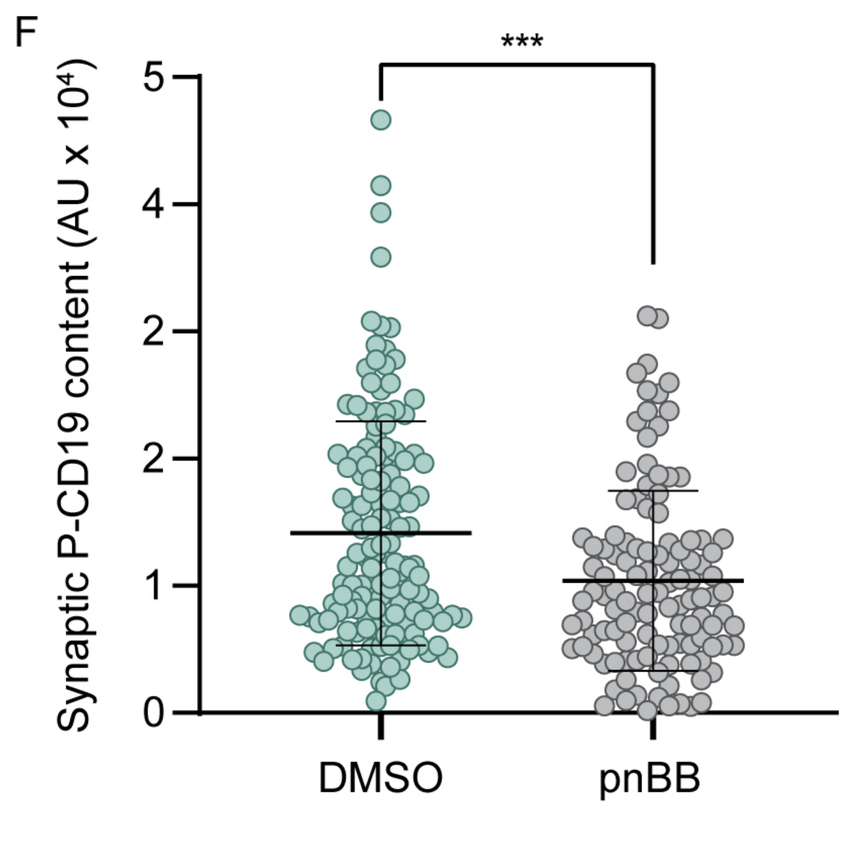

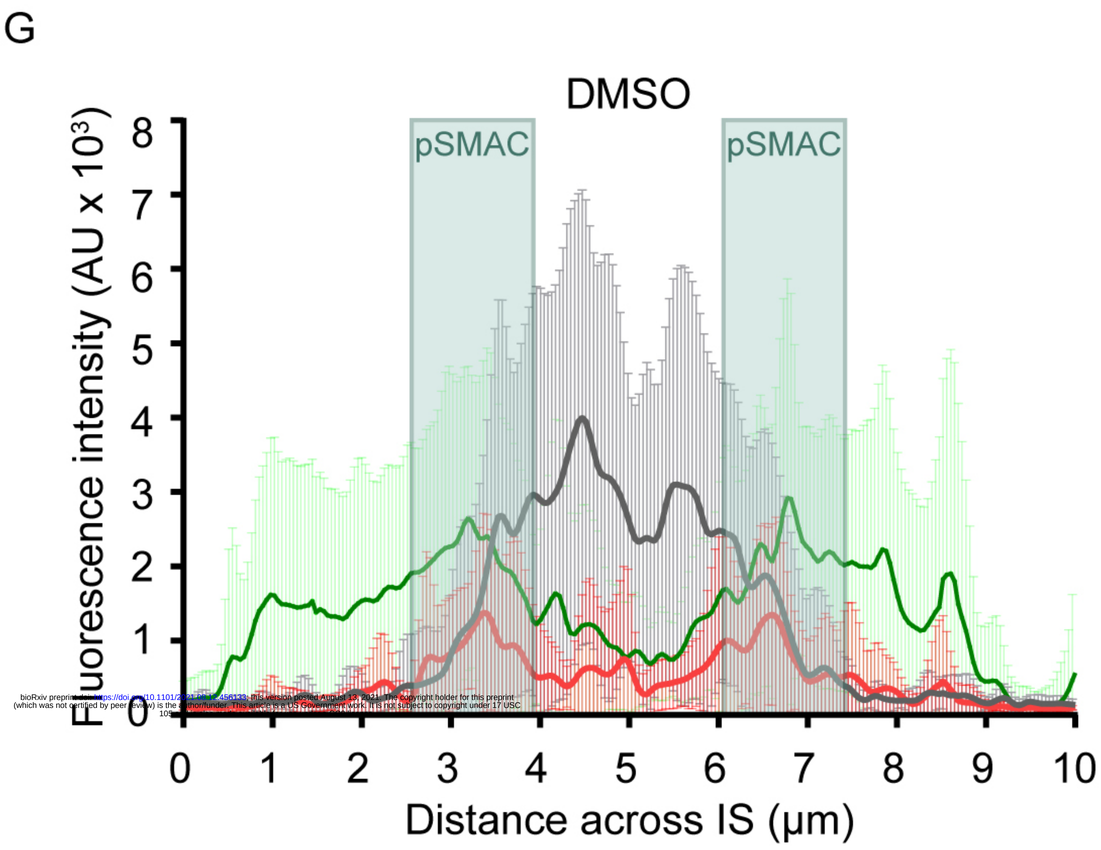

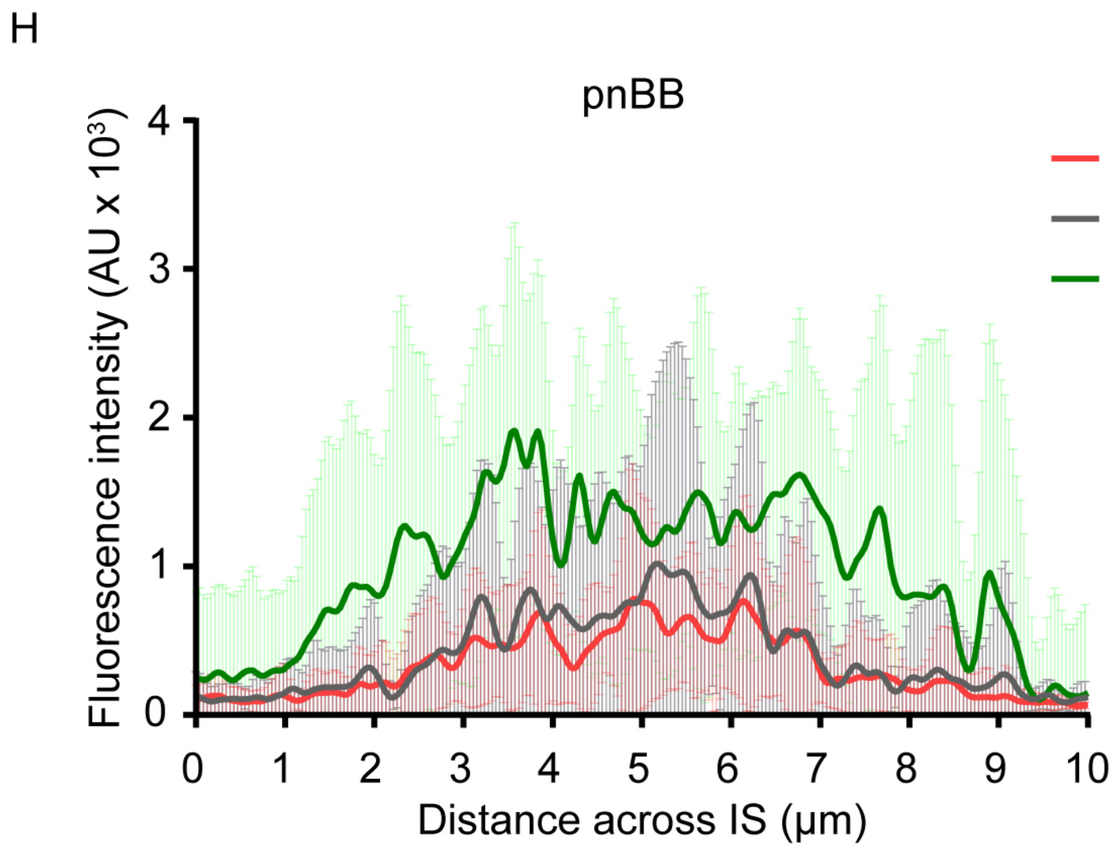

Figure 7